Princetonlaan 6
3584 CB Utrecht
P.O. Box 80015
3508 TA Utrecht
The Netherlands

www.tno.nl

T +31 88 866 42 56
F +31 88 866 44 75

TNO report

TNO2021_R11382

Cavern convergence and subsidence: assessment of the Heiligerlee cavern field

Date	28 July 2021
Author(s)	Jaap Breunese, Peter A. Fokker, Bogdan Orlic†, Serge van Gessel
Reviewer(s)	Prof. dr. Christopher J. Spiers (UU), Ingrid Kroon (TNO-AGE)
Copy no	
No. of copies	
Number of pages	74
Number of appendices	0
Sponsor	Staatstoezicht op de Mijnen
Project name	Heiligerlee Bodemdaling
Project number	060.43341/01.14

Samenvatting

Aanleiding
Staatstoezicht op de Mijnen (SodM) houdt toezicht op de sluiting en abandonnering van zoutcavernes binnen de zoutproductielocatie Heiligerlee. Hiervoor is aanvullende kennis en inzicht nodig omtrent de factoren en specifieke scenario's voor sluiting die de ontwikkeling van lange-termijn bodemdaling bepalen. De inzichten hebben ook implicaties voor cavernesluiting op andere locaties en geven richting aan het oplossen van resterende kennisvragen.

Onderzoeksvraag
Op verzoek van SodM heeft TNO-AGE analyses uitgevoerd op het mogelijke verloop van toekomstige bodemdaling bij de Heiligerlee zoutproductielocatie (noordoost Nederland). Hierbij zijn verschillende scenario's voor de cavernedruk na sluiting geëvalueerd (variërend tussen halmostatische druk en 90% van de lithostatische druk). Bij het onderzoek is aangenomen dat de 12 cavernes simultaan en volgens eenzelfde drukregime worden gesloten. De specifieke doelstellingen van de studie zijn:

- Het bepalen van de invloed van drukregimes na sluiting op de verwachte snelheid en ontwikkeling van caverneconvergentie en bodemdaling voor verschillende scenario's tussen halmostatische druk en 90% lithostatische druk.
- Het bepalen van de verwachte totale bodemdaling op het diepste punt van de bodemdalingskom bij de Heiligerlee productielocatie binnen een voorspellingstermijn van 50 jaar. Hierbij worden ook inzichten gegeven in de beperkingen ten aanzien van het berekenen van bodemdaling op lange-termijn tijdschalen.
- Het geven van inzichten in de belangrijkste onzekerheden en gevoeligheden (anders dan de gebruikte drukscenario's) die invloed hebben op de bodemdalingsvoorspellingen.

Aanpak modellering
Om antwoord te geven op de specifieke vragen en doelstellingen in deze studie, zijn de volgende, onderling samenhangende modellen ontwikkeld:

- Een DIANA model voor één enkele zoutcaverne. Dit model staat centraal bij het integraal onderzoeken van zowel de caverneconvergentie als daaruit voortvloeiende bodemdaling;
- Een special voor deze studie ontwikkeld analytisch model voor één enkele zoutcaverne. Dit model is primair gebruikt om snel gevoeligheden door te rekenen die samenhangen met toegepaste cavernedruk en zoutkruip-reologie
- Een numeriek multi-caverne *plane-strain* model dat gebruikt is om de invloed van geomechanische interacties tussen cavernes op het algemene deformatie gedrag te onderzoeken.

Modellering van zoutkruip
In deze studie is naast de traditionele 'power-law' zoutkruip ook een lineaire zoutkruip meegenomen als component in de bepaling van caverneconvergentie. Lineaire zoutkruip is tot dusverre zelden toegepast bij praktische engineering

studies zoals Heiligerlee. Deze component heeft echter mogelijk een belangrijke invloed in lange-termijn scenario's waarin zoutcavernes onder verhoogde druk worden gehouden. De gebruikte modellen zijn aangepast en volledig afgestemd op het toepassen van een combinatie van power-law en lineaire zoutkruip.

De toevoeging van lineaire zoutkruip in cavernemodellen wordt beschouwd als een mogelijk belangrijke, maar tegelijkertijd ook onzekere parameter. Deze onzekerheid hangt o.a. samen met de beperkte toegankelijkheid tot experimentele (lange-termijn) tests gericht op het bepalen van lineaire zoutkruip. In deze studie wordt derhalve een ruime onzekerheidsbandbreedte aangenomen voor deze parameter.

Vergelijk met velddata
De introductie van lineaire zoutkruip in de modellering heeft geresulteerd in een grote bandbreedte van mogelijke convergentie- en bodemdalingssnelheden. Veel van de uitkomsten zijn significant hoger dan wat tot nu gemeten is in veldobservaties. Een belangrijk punt hierbij is dat de afstand waarop lineaire zoutkruip bijdraagt (drempelwaarde) een zeer grote invloed heeft op de gemodelleerde convergentiesnelheden. Deze afstand is hier ingegeven door de afgebakende omvang van de Winschoten zoutpijler binnen het Heiligerlee gebied, maar kan ook worden gezien als een representatie van de intrinsieke drempelwaarde voor lineaire zoutkruip bij zeer lage deviatorische spanningen.

De gemodelleerde bodemdalingssnelheden uit deze studie zijn vergeleken met gegevens uit beschikbare PS-InSAR metingen. Hieruit blijkt dat de combinatie van lage lineaire zoutkruip en een bijbehorende effectieve invloedsradius van 500 meter het beste aansluit bij de observaties.

In het geval dat de effectieve radius een intrinsiek gegeven is voor lineaire zoutkruip, dan moet worden opgemerkt dat de combinatie van beide parameters niet uniek is. Een combinatie van grotere bijdrage van lineaire zoutkruip en een kleinere radius van invloed zou eveneens de geobserveerde convergentie en bodemdaling kunnen verklaren. N.B.: De toepassing van zoutkruipwaarden op de Heiligerlee casus, zoals gegeven door Prof. Spiers (0,07 – 0,7 MPa, pers.comm 30-11-2020), corresponderen met een radius (drempelwaarde) in de orde van enkele honderden meters. Dit houdt in dat een grotere invloed van lineaire zoutkruip (zoals aangenomen in de 'low case') niet kan worden uitgesloten.

Resultaten
De toekomstige convergentie- en bodemdalingssnelheden voor de verschillende caverne-drukscenario's zijn berekend op basis van het best-passende model. Hiermee zou de cumulatieve bodemdaling op het diepste punt van de dalingskom over een periode van 50 jaar na sluiting uitkomen op 31±11 cm en 22±7 cm voor respectievelijk het halmostatische en het 90%-lithostatische drukscenario. Deze waarden moeten worden opgeteld bij de reeds opgetreden bodemdaling van 18 cm die is opgetreden sinds aanvang van de zoutproductie.

Discussie
De studie laat zien dat het introduceren van lineaire zoutkruip in de geomechanische modellering de caverne-drukafhankelijkheid van convergentie aanzienlijk vermindert. Dit effect is aangetoond voor de periode van 50 jaar na een sluiting en regulering van cavernedruk. Verder zal de interactie tussen cavernes,

zoals gemodelleerd in dit rapport, aanzienlijk minder blijken te zijn wanneer een drempel in de lineaire kruip wordt geïntroduceerd.

We willen benadrukken dat de modelleringsaannames die tot deze resultaten leiden, verdere wetenschappelijke bevestiging nodig hebben, zowel theoretisch als uit experimenten. Dit raakt mogelijk aan de uitkomsten van langdurige discussies over de rol van lineaire zoutkruip op verschillende ruimtelijke en tijdschalen (lab, mijnbouwkunde, tektoniek).

Aanbevelingen

- Voer een kritische wetenschappelijke beoordeling uit van de onderliggende modelleringsaannames. De herziening zou zich met name moeten richten op de impact van lineaire zoutkruip, inclusief de fysieke drempel en het bijbehorende ruimtelijke bereik voor de deviatorische spanning voor lineaire kruip die vanuit een fundamenteel natuurkundig oogpunt wordt verondersteld te bestaan.
- Voer een inverse studie uit op de geodetische signalen (InSAR en benchmarks) om de bijdragen van zoutcaverne-gerelateerde operaties, het Groningen-gasveld en andere (autonome) bronnen te ontrafelen. Een dergelijk onderzoek zou zich moeten richten op het beter bepalen van de caverne-convergentiesnelheid in samenhang met de sturende geomechanische parameters. Dit zou de historische vergelijking van geomechanische modellering met observaties verbeteren, vooral omdat in de Heiligerlee casus het in-situ convergentievolume niet met benodigde (praktische) nauwkeurigheid kan worden gemeten en evenmin kan worden afgeleid uit de massabalans.
- Overweeg om de toegevoegde waarde en de praktische haalbaarheid van de hier onderzochte 'zachte insluitings'-methode in vergelijking met de traditionele ‘harde insluitings’-methode.
- Ontwikkel een monitoringprogramma dat de in dit onderzoek bepaalde bodemdalingsprognoses kan valideren (of verwerpen en verbeteren).

Summary

Motivation of the study
To support their supervision on cavern closure at the Heiligerlee salt production location, State Supervision of Mines (Dutch abbreviation: SodM) requires additional knowledge and understanding on factors and specific closure schemes controlling the progress of long-term subsidence. The insights can have implications for cavern closure at other locations as well and provides directions on the remaining key research questions to be solved.

Research question
At the request of SodM, TNO-AGE has analysed post-closure subsidence forecasts at the Heiligerlee salt production location (northeast Netherlands), considering different pressure conditions from halmostatic to 90% lithostatic pressure. The assessment follows the assumption that the 12 caverns are immediately and simultaneously put on pressure control via the wells. The specific study objectives are to assess:

- The influence of post-closure pressure regimes on the expected rate and progression of cavern convergence and subsidence using a range between 90% lithostatic pressure[1] and halmostatic pressure;
- The development of expected total subsidence at the deepest point of the subsidence bowl at the Heiligerlee location within a 50-year forecast window, including insights and limitations to assess the subsidence on long-term time scales.
- The key uncertainties and most important sensitivities, other than deterministic post-closure pressure scenarios, that influence these subsidence predictions.

Modelling strategy
In order to meet the objectives, we have developed a modelling strategy using a suite of geomechanical models, that were developed for the purpose of this project:

- a single cavern DIANA model, being the central tool for studying both cavern convergence and subsidence in an integrated manner;
- an analytical single cavern convergence model, primarily used as a fast model for studying sensitivities on cavern pressure and salt creep rheology;
- a numerical multi-cavern plane strain model aimed at estimating the impact of geomechanical interactions between the caverns on their overall deformation behaviour.

Salt creep modelling
We have chosen to extend the traditional ‘power law only’ approach to also include linear salt creep. The latter has rarely been applied to real case engineering problems, such as Heiligerlee. Linear creep may be important in long term pressure control scenario’s at elevated cavern pressures. Our suite of models was therefore fully geared to an integrated approach of a combination of power law and linear salt creep.

[1] Note that this study does not investigate what pressure level can be considered as “safe pressure”. The 90% lithostatic level is chosen in communication with SodM.

The contribution of linear creep was considered both a potentially important, but also quite uncertain parameter. The uncertainty pertains to the difficult experimental accessibility of linear salt creep (very long tests). Therefore, we defined a rather broad *a priori* range of uncertainty for that parameter.

Comparison with field data
The introduction of linear creep into our modelling has resulted in a large range of possible convergence and subsidence rates, most of them at much larger values than have been observed in the field. Importantly, the introduction of a spatial range (threshold) for linear salt creep turned out to have a very significant reducing effect on the modelled rates. Such a spatial range was inspired by the finite extrinsic physical size of the Winschoten salt dome (cf. Chapter 2) but could also be seen as the representation of an intrinsic threshold for linear creep at very low deviatoric stresses.
We compared our modelled subsidence rates to the ones as observed from PS-InSAR. The combination of Low linear creep and a 500-meter effective radius for the linear creep was found to comply best with the observations.

Should the effective radius be an intrinsic salt creep feature, please note that this parameter combination is not unique: a combination of higher contribution from linear creep with a smaller radius might explain the convergence and subsidence rates equally well (and vice versa). In fact, applying the range provided by prof. Spiers (0.07 – 0.7 MPa, personal communication 30-11-2020) to the Heiligerlee case corresponds to spatial ranges for linear creep in the order of hundreds of meters. Therefore, it cannot be excluded, that linear creep intrinsically is stronger than assumed in the Low case.

Results
Using the best matching model, the future convergence and subsidence rates were calculated for the prescribed pressure control scenarios. A horizon of 50 years would yield cumulative subsidence of 31±11 cm and 22±7 cm at the deepest point of the subsidence bowl for the halmostatic case and the case with cavern pressure 90% of the virgin stress, respectively. These numbers must be added to the subsidence already induced during the production phase of the cavern field, which now is in the order of 18 cm.

Discussion
We have observed that introducing linear creep into the geomechanical modelling does relax the cavern pressure dependence of convergence significantly. We have shown this effect for the 50 years period following a pressure control mode of operation. Further, the interaction between caverns, as modelled in this report, will turn out to be significantly less, when a threshold in the linear creep is introduced.

We like to stress that the modelling assumptions leading to our results need further scientific confirmation, both theoretically and from experiments. They possibly touch at the resolution of a long-standing discussion of the role of linear salt creep at various spatial and time scales (lab, mining engineering, tectonics). This has led us to the recommendations stated below.

Recommendations

- Perform a critical scientific review as to the underlying modelling assumptions. The review should target in particular the impact of linear salt creep, including the physical threshold and associated spatial range for the deviatoric stress for linear creep supposed to exist from a fundamental physics point of view.
- Perform an inverse study on the geodetic signals (InSAR and benchmarks) in order to unravel the contributions from salt cavern related operations, the Groningen gas field and other (autonomous) sources. Such a study should target to better determine the cavern squeeze rate along with the driving geomechanical parameters. This would enhance the history match of the geomechanical modelling, especially since in the Heiligerlee case convergence volume is not measurable in-situ with any practical accuracy nor can it be derived from mass balance considerations.
- Consider the added value and the practical feasibility of the ‘soft shut-in’ method approach investigated here when compared to the traditional hard shut-in method.
- Develop a monitoring program, that can validate (or reject and improve on) the subsidence projections made in this study.

Contents

1 Introduction

This study addresses long term subsidence due to cavern closure under different closure conditions at the Heiligerlee salt production location, northeast Netherlands.

1.1 Rationale and background

To support their supervision on cavern closure at the Heiligerlee salt production location, State Supervision of Mines (Dutch abbreviation: SodM) requires additional knowledge and understanding on factors controlling the progress of long-term subsidence.

The current cavern closure guideline aims at realizing a hard shut-in. Over the past years concerns have been expressed regarding the potential risks of abandoning caverns at high pressures[2, 3, 4, 5]. These concerns have been intensified after recent pressure drop and brine escape incidents at caverns in the Barradeel and Veendam salt production concessions[6]. For this reason, alternative closure options are being evaluated, in which the cavern volume remains accessible via a suspended well (soft shut-in) in order to control pressure by periodically releasing brine.

Against this background, the following research questions have been formulated to focus the investigation:

- How will closure at different abandonment pressures control the rate of cavern convergence and subsidence at the Heiligerlee caverns;
- What is the expected total subsidence of all 12 caverns at the Heiligerlee location on the long term after closure, given the available data and knowledge;
- How and to what extent will the results and insights from this research be applicable to assess cavern closure strategies at other locations.

1.2 Study objectives and scope

This study addresses long term subsidence due to cavern closure under different pressure conditions at the Heiligerlee salt production location, northeast Netherlands. The assessment follows the assumption that the 12 caverns are immediately and simultaneously closed using the soft shut in approach, while considering two end member states. In the first, the cavern is kept under a pre-determined maximum pressure, while releasing minimal amounts of brine. In the

[2] Rokahr, R.B., Hauck, R., Staudtmeister, K., Zander-Schiebenhofer, D., Crotogino, F. & Rolfs, O. (2002). High pressure cavern analysis. SMRI report no. 2002-2-SMRI, 88 p.
[3] Pruiksma, J.P. (2005). Shut-in gedrag en stabiliteit FRISIA caverne, FEM berekeningen en kruipgedrag. Delft: Deltares, Report No. CO-400132-0006
[4] Lux, K.-H. & Wolters, R. (2010). Untersuchung der konvergenzinduzierten zeitlichen und räumlichen Soleinfiltration aus der Kaverne BAS-3 in das anstehende Steinsalzgebirge, Clausthal
[5] Bérest P. & Brouard, B. (2003). Safety of Salt Caverns Used for Underground Storage Blow Out; Mechanical Instability; Seepage; Cavern Abandonment. Oil & Gas Science and Technology 58(3):361-384. DOI: 10.2516/ogst:2003023
[6] Fokker, P.A. (2018), "Managing pressures in Nedmag caverns to prevent brine leakage during the mining and bleed-off phase and an evaluation of post abandonment cavern behaviour." (available from www.nedmag.nl)

second, the cavern well is open and brine can freely flow out with increasing cavern convergence (halmostatic pressure condition).

The study objectives are to investigate:

- The influence of post-closure pressure regimes on the expected rate and progression of cavern convergence and subsidence using a range between 90% lithostatic pressure[7] and halmostatic pressure;
- The development of expected total subsidence at the deepest point of the subsidence bowl at the Heiligerlee location within a 50-year forecast window, including insights and limitations to assess the subsidence on very long-term time scales (see ad.1).
- The key uncertainties and most important sensitivities, other than post-closure pressure, that influence these subsidence predictions (see ad.2).

Ad.1: At start of this project “long term” was defined as the period it takes the cavern to converge to a volume of 10% of the volume at the moment production ends. During the analysis and modelling it became apparent that, given the available site-specific data and prior evaluations, it is not possible to provide a reliable and scientifically justified estimation at this timescale, i.e.:

- The uncertainties in several important aspects of the modelling process prevent an estimation within reasonable (and explanatory) confidence ranges. These include among others the salt creep parameters, the subsidence influence functions and other factors controlling the shape of the subsidence bowl, the 3D model complexity of the laterally confined salt body, and the unpredictable cavern volume interactions at advanced levels of convergence.
- Beyond a certain level of cavern convergence, the applied finite element models yield anomalous results as squeezing and deformation results in inconsistent cell geometries.
- A comprehensive history match was lacking and not feasible within the project scope.

For the above reasons and with the progressing insights from the modelling results, it was decided to limit the subsidence predictions to a 50-year period after assumed cavern closure. Recommendations for future improved long-term predictions are provided.

Ad.2: At the start of this study the focus was put on the influence of the different (i.e. linear and non-linear) components of the salt creep model. At a later stage, the influence of salt formation geometry and cavern distribution was investigated as well. It should be noted that these aspects impacted the applicability of the developed analytical model and finite element model. For this reason, several pragmatic modelling choices and simplifications had to be made.

The following scope definitions apply:

- The study evaluates the subsidence effects as a result of the periodic release of brine and consequent salt creep and cavern convergence. Other aspects, such as fracture formation, brine permeation, cavern or well integrity, are not part of the study.

[7] Note that this study does not investigate what pressure level can be considered as “safe pressure”. The 90% lithostatic level is chosen arbitrarily in communication with SodM.

- Literature research is focused on studies that directly pertain to the Heiligerlee situation.
- The study focuses on the effects of salt creep and cavern convergence in terms of subsidence. The local impacts of subsidence and eventual hazard levels are not included in the investigation.
- All models and calculations are carried out based on the available data and information, as confirmed and agreed by SodM.
- Salt creep and cavern convergence are estimated under the assumption that all caverns are simultaneously closed at the latest reported volume. A uniform pressure regime is considered for all 12 caverns in the Heiligerlee concession.
- The study does not determine what pressure maintenance levels can be considered as “safe”. The chosen pressure levels in the subsidence scenarios are solely defined to investigate the influence on subsidence rates.

1.3 General approach and report structure

Salt creep is the basic driving mechanism for time-dependent deformation around salt caverns, reaching the surface as subsidence. On this topic there is a vast amount of literature, including recent studies on the Heiligerlee location. We use this information as a starting point for our work. In order to estimate subsidence for individual caverns we use two models. One is a newly developed, fast analytical model that considers different salt creep model components (including a combination of power law creep and linear creep as a description of salt creep). The second is a numerical model developed in the DIANA software (DIANA FEA, 2020) that is used to validate the analytical solution, to determine the subsidence influence functions and to assess the impact of nearby caverns and constraints of the salt dome geometry. Using the derived, final subsidence rates of individual caverns, the combined subsidence from the 12 Heiligerlee caverns is estimated. Sensitivities are investigated using different parameters for the salt creep model and influence functions.

The report structure is as follows.

Chapter 2 provides a technical description of the Heiligerlee cavern field.

Chapter 3 summarizes the research in earlier studies and details the proposed modelling strategy in this study.

Chapter 4 explains the applied constitutive models for salt creep, the parameter choices and inherent uncertainties, limitations and unknowns.

Chapter 5 presents the single-cavern numerical model and the single-cavern results for the various pressure scenarios.

Chapter 6 introduces the newly developed, analytical model for single cavern convergence. The chapter concludes with a validation of this analytical model using the numerical model results.

Chapter 7 presents the multi-cavern numerical model and multi-cavern results.

Chapter 8 assesses the subsidence results from Chapter 7 for the period between start of cavern development and present state. This assessment is used to define the preferred parameters and boundary conditions for the subsidence forecasting.

Chapter 9 presents the final subsidence forecast results for the different cavern closure conditions, including a comparison with the subsidence forecast based on subsidence rated obtained from the DEEP-KBB study.

Chapter 10 draws the conclusions from the modelling, including recommendations to reduce uncertainties and address remaining research questions.

2 Description of the Heiligerlee salt cavern cluster

AKZO Nobel (currently Nobian) has started the development of salt caverns in the Heiligerlee salt dome in 1956 (Adolf van Nassau production licence). Since then 12 salt caverns (HL-A to HL-M) have been leached, including one storage cavern for nitrogen gas (HL-K) operated by Gasunie. The produced salt interval is located on top of the south-eastern margin of the Groningen gas field.

Figure 2-1 shows the location of the Winschoten salt structure relative to other salt domes. Figure 2-2 shows a more detailed map of the Heiligerlee area and the location of the salt caverns. Figure 2-3 illustrates the local geological situation in cross section.

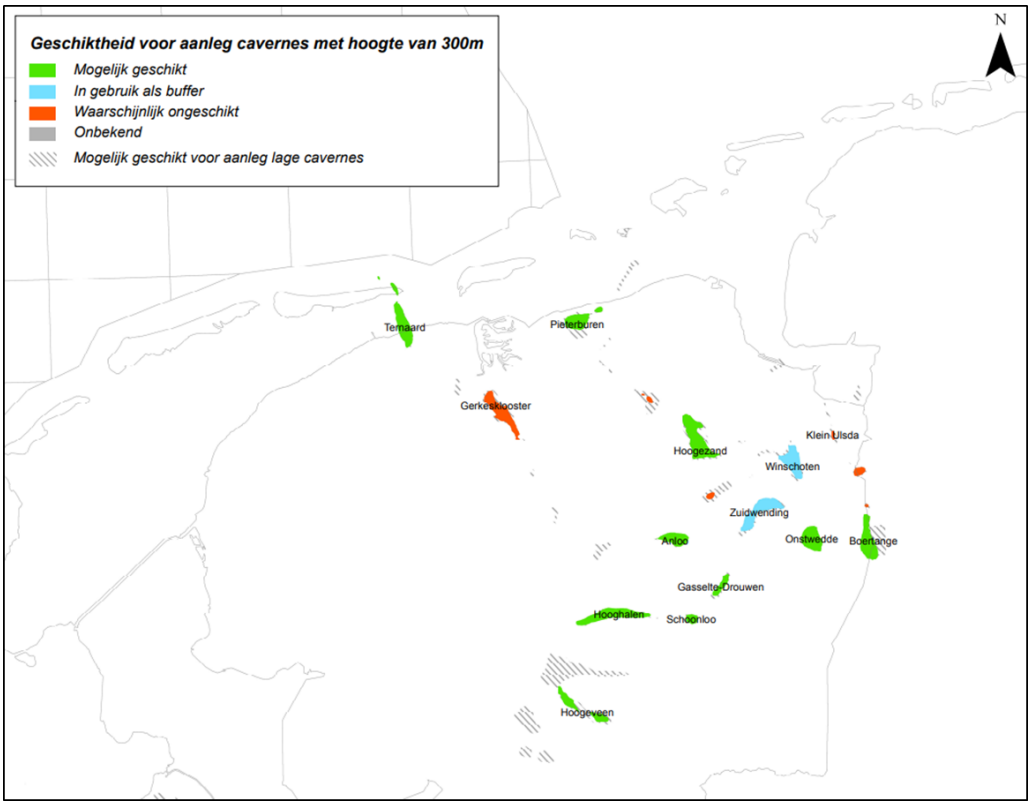

Figure 2-1: Overview map of salt structures and the location of the Winschoten salt dome in northeast Netherlands (TNO-2014).

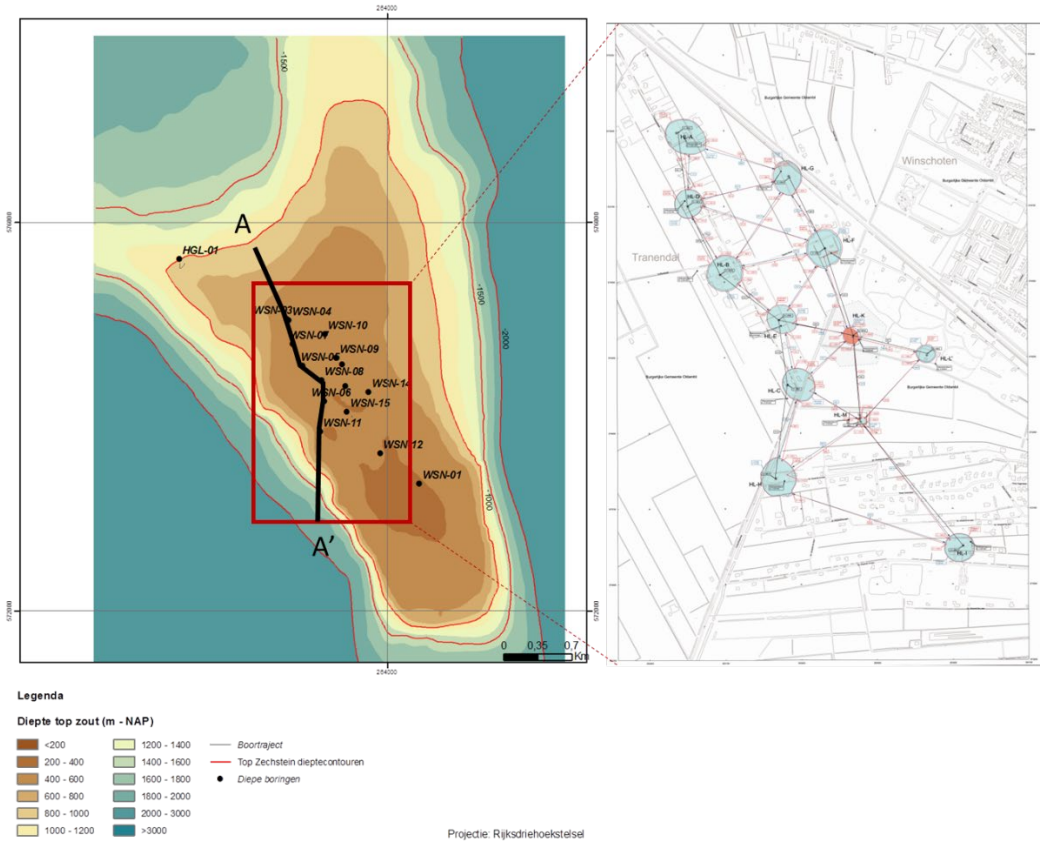

Figure 2-2: Location map of the Heiligerlee salt dome with depth top Zechstein (left) and location of existing 12 caverns (right).

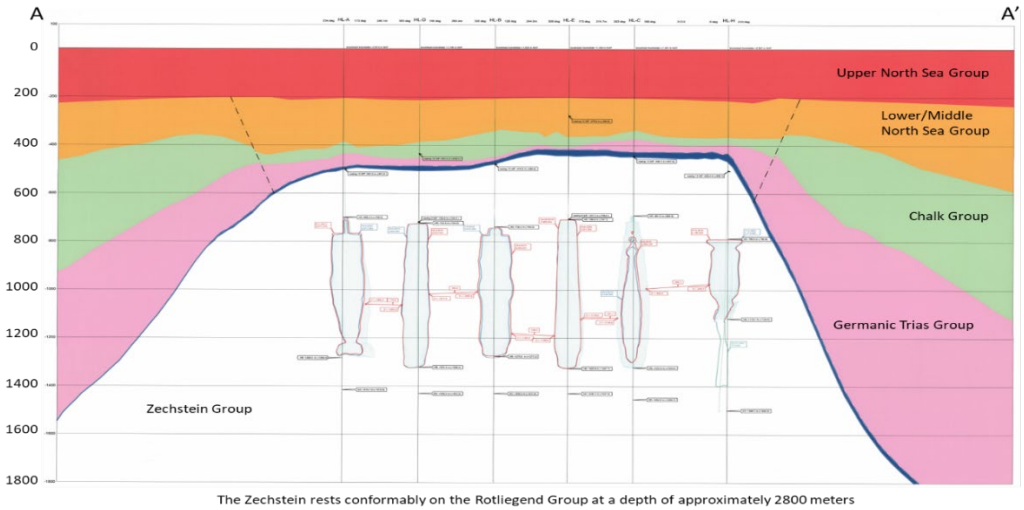

Figure 2-3: Geological cross section with location of caverns. Trajectory A-A' is shown in Figure 2-2 (After Akzo Nobel, 2004[8]).

[8] Akzo-Nobel 2004: Caverneveld Heiligerlee, doorsnede 1

The caverns are situated in rock salt deposits of the Strassfurt (Z2) series in the Zechstein Group. The flanks of the dome are steep and defined by younger Zechstein formations. Laterally the salt dome lies adjacent to sandstones and claystones of the Germanic Trias Groups. Directly above the salt dome there is an overburden consisting predominantly of Cenozoic sand and clay deposits. The top of the Zechstein Group is located at a depth of ca. 450 m while the base of the Zechstein rests conformably on Rotliegend sandstones and claystones at a depth of ca. 2800 m.

The rock salt in the Winschoten dome is very pure (>96 % NaCl) with minor (<1%) admixture of other minerals (anhydrite, poly-halite, kieserite, sylvite). No kalium-magnesium layers, floaters or gas pockets are encountered in the drilled sections.

Up to 2015 almost 70 million tonnes of salt have been dissolved, leaving a gross cavern volume of ca. 33 million m^3. Table 2-1 shows the general production data and geometrical characteristics of each cavern.

Table 2-1: Overview of cavern general parameters and characteristics.

Cavern	Status	Prod. Start (year)	Prod. End (year)	Depth Top Salt (m)	Depth Top Cavern (m)	Depth Base Cavern (m)	Radius (m)	Cavern Volume (m. m^3)
HL-A	Producing	1956		500	750	1250	52.1	4.27
HL-B	Suspended	1956	2016	480	750	1275	50.7	4.23
HL-C	Producing	1958		450	700	1320	43.6	3.70
HL-D	Producing	1958		500	720	1320	39.7	2.97
HL-E	Suspended	1958	2002?	440	710	1325	39.2	2.97
HL-F	Producing	1962		450	850	1345	48.7	3.70
HL-G	Suspended	1964	1997?	450	900	1370	35.4	1.85
HL-H	Suspended	1964	2005?	450	790	1400	33.8	2.19
HL-I	Producing	1966		425	800	1330	39.1	2.55
HL-K	Gas storage	1996	2016	450	1025	1500	23.5	0.82
HL-L	Producing	1999		450	1100	1510	28.4	1.04
HL-M	Producing	2005		425	1400	1625	20.6	0.07

3 Modelling strategy

Below, first the most recent studies on Heiligerlee are summarized. Then their technical limitations are discussed, leading to the modelling strategy that we have applied in this project.

3.1 Recent research on Heiligerlee (and Zuidwending)

3.1.1 Analysis KBB studies Heiligerlee and Zuidwending 2015

In 2015 Akzo Nobel requested the German consultant KBB to produce several studies (hereafter KBB-2015) on the convergence and subsidence behaviour of the cavern fields in order to fulfil the requirements of the state supervision of mines for a history matched model, that could be used in a predictive mode. KBB has produced reports for the Heiligerlee[9] and for the Zuidwending cavern field[10] using comparable approaches.

3.1.2 Analysis IfG study Zuidwending 2016

A year later Gasunie requested IfG (hereafter IfG-2016) to study the convergence behaviour of the storage cavern under operational conditions typical for the storage operation[11]. Marked differences with the salt mining caverns are the storage caverns are smaller and the internal pressure is cyclic rather than constant. Subsidence was out of scope in this study.

3.2 Limitations of earlier work on Heiligerlee / Zuidwending

3.2.1 KBB 2015[9]

TNO has observed the following with respect to the KBB-2015 study:

Cavern volume

To derive the development of the volume of the individual caverns over time KBB used material balance information. This seems sufficiently constrained by sonar measurements. The deviations between calculated and measured cavern volumes generally are in the order of a few percent (see KBB-2015 WP2, Enclosures 4-15). Note that no geomechanical model has been involved here.

Convergence

Cavern convergence under operational (i.e. near halmostatic) conditions has been modelled using only an analytical power law Norton-Hoff type salt creep response model (Eq. 3.3 in KBB-2015). Enclosure 3 from the KBB-2015 report shows the assumed creep response (without further justification from e.g. lab data).

It is noted that the volume convergence rate as derived by KBB is so small (order of 0.1% per year), that it cannot be derived from the combination of sonar and mass

[9] KBB (2015). Prediction of Subsidence above Caverns at Heiligerlee, The Netherlands Operation Phase Report on WP2: Applied Subsidence Model Report for Akzo-Nobel (31-8-2015)
[10] KBB (2015). Prediction of Subsidence above Caverns at Zuidwending, The Netherlands Operation Phase Report on WP2: Applied Subsidence Model. Report for Akzo-Nobel (31-8-2015)
[11] IfG (2016). Rock Mechanical Modelling (incl. history and surrounding caverns) of the Nitrogen Storage Cavern HL-K at Heiligerlee, The Netherlands. Report for Gasunie (28-6-2016)

balance information with any practical accuracy[12]. Therefore, by lack of other information, KBB in effect did derive cavern convergence rates from subsidence analysis and its associated uncertainties, as is described below.

Subsidence

KBB has modelled subsidence as follows:

- *A priori* take the shape of the subsidence bowl of a single cavern to be a Gaussian bowl, with a parameter β allowing for lateral broadening of the bowl over time, see Eq. 3.1 in KBB-2015;
- *A priori* assume that the convergence volume of a cavern is equal to the volume of the subsidence bowl it creates (KBB: bulking factor a = 1).

This modelling approach oversimplifies the geomechanical connection between cavern convergence and surface deformation. This is an important aspect when trying to come to a predictive model, in particular when the prediction pertains to different operational conditions (e.g. cavern pressures) than in the past.

As for the benchmark data:
KBB notes, that subsidence over the Heiligerlee cavern fields is caused by the sum of contributions from 1) the salt mining (and storage), 2) gas production from the underlying Groningen field, and 3) autonomous (i.e. not mining related) causes. The contribution from autonomous sources is relatively small, which seems justified in a high-quality network of founded benchmarks. However, the contribution from the Groningen field, as taken from subsidence maps from NAM is reported to be of the same order of magnitude as that from the Heiligerlee caverns over de epochs studied[13]. As a result, KBB has corrected the benchmark signals for a considerable amount in order to arrive at the signal that is supposed to come from the salt cavern operations only. The KBB report shows, that the derived salt signal is of the same order as the uncertainty in that signal: this introduces quite a large uncertainty in the derived convergence rate and volumes too.

3.2.2 IfG 2016

IfG has studied the geomechanical behaviour of the gas storage salt cavern HL-K. The driver for this study was a leak detected in the storage well. The numerical modelling used the ‘Lubby-2’ salt creep constitutive law, which is a marked difference with the KBB 2015 study (where subsidence was out of scope). It also included interaction with the nearest salt mining cavern HL-E.

3.3 Current modelling strategy

3.3.1 Model choices

Salt creep is the basic driving mechanism for time dependent deformation around salt caverns, reaching the surface as subsidence. There is a vast amount of literature on theoretical and experimental treatment of salt creep. From the theoretical side, salt creep is a physically complex phenomenon, usually described by empirical constitutive laws. From the experimental side, salt creep is difficult to

[12] Note: in IfG-2016 this was possible due to the much higher convergence rates under operational conditions in the order of 50% per year in that case.
[13] This is likely to have been the case over the full history starting in the 50’s, since the Groningen gas production and the Heiligerlee salt production have followed a similar time line.

assess. This is mainly because of the relatively small displacements and very slow displacement rates under practical laboratory conditions.

Salt creep constitutive model

KBB has used the classical Norton-Hoff power law as the constitutive equation to describe cavern convergence. In our view a combination of power law creep and linear creep would be a more appropriate description of salt creep. This choice was inspired by both theoretical work and laboratory experiments. In addition, experimental evidence - if not proof - of linear creep has come from long-duration very slow creep tests on natural salt samples, executed in abandoned salt mines under well controlled temperature, pressure and moisture conditions. The salt creep model is described in detail in **Chapter 4.**

Single cavern FEM

The FEM software DIANA, developed by TNO, has the combination of power law and linear creep as a standard option. It was used to construct a model of a typical cavern in the Heiligerlee setting. This model is described in detail in **Chapter 5** and has many functions in this project, such as studying:

- Cavern convergence as a function of the assumed salt creep law, in particular the linear creep contribution;
- The convergence as a function of the pressure in the cavern;
- The associated subsidence over the cavern;
- The impact of the finite size of the salt dome in which the Heiligerlee cavern field is situated, both on cavern convergence and on subsidence.

Analytical single cavern convergence model

An analytical expression was deemed useful to perform fast sensitivity analyses on parameters (such as the contribution of linear creep and the controlled internal cavern pressure). Moreover, an analytical solution would readily allow for upscaling of single cavern solutions to the multi-cavern setting at Heiligerlee. This kind of upscaling is a fast alternative to complex, time-consuming, three-dimensional numerical modelling of multiple caverns in a dome-scale models[14]. Therefore, an analytical solution was developed within the framework of this study. Its derivation is presented in **Chapter 6**. To the best of our knowledge, such a solution has not been published before.

Thus, the DIANA model results also served as a benchmark for this analytical solution of cavern convergence and to generate influence functions, to be used to translate cavern convergence into subsidence in an analytical fast manner (see next Chapters).

[14] Sobolik, S.R. & Ehgartner, B.L. (2012). Analyzing large pressure changes on the stability of large-diameter caverns using the M-D model. Mechanical Behavior of Salt VII - Proceedings of the 7th Conference on the Mechanical Behavior of Salt. 321-329. 10.1201/b12041-44.

Numerical 2D multi cavern model for convergence interaction

The Heiligerlee concession comprises 12 caverns. One of the questions pertains to their interference: can the effect of the cavern field be established through the summation of the fields resulting from single, isolated ones? In other words, does the existence of a nearby cavern change the behaviour of the other caverns?

Chapter 7 describes a geomechanical plane-strain model of a horizontal cross-section at half depth of multiple salt caverns. Aim of this 2D plane strain modelling is to estimate convergence rates of caverns of different sizes and the stress profiles between interacting caverns. The limitation of the plane-strain model is that it cannot predict surface deformation. If, however, the superposition principle applies to the 2D calculation with multiple caverns we are building confidence that it also applies for the 3D cavern field. A full 3D numerical calculation was outside the scope of the present project.

3.3.2 Potential improvements with respect to the existing Heiligerlee modelling

During the design of the modelling instruments described above, we have been well aware that these choices add more complexity to the existing model of KBB, and we would run the risk of encountering surprises. But the need for this modelling strategy was motivated by our goal to better understand the long-term convergence and subsidence behaviour, under operational conditions that have not existed so far, e.g. higher than halmostatic cavern pressures. This is at the heart of the research objective.

To summarize, the potential improvements that we envisaged were:

- Create a predictive subsidence model, that integrates cavern convergence and surface deformation (rather than treat these separately and largely uncoupled);
- Explicitly take linear salt creep, and its uncertainty, into account in the integrated modelling (rather than only use power law creep), which in our view is crucial to understand the long-term behaviour of the cavern system under various controlled pressure conditions;
- Use a combination of numerical and analytical tools that allows for upscaling of single cavern solutions to the multi cavern setting and for fast sensitivity analyses on parameters;
- Investigate the effect of the finite size of the salt dome.

4 Salt creep modelling

4.1 Constitutive laws and their parameters

4.1.1 Motivation to study the role of linear viscoelasticity

It is generally accepted, that the rheology of rock salt is very complex. Under typical mining operation conditions, cavern convergence has traditionally been described by a power law type relationship between strain rate and stress. However, over the last decades both theoretical and experimental evidence has piled up indicating the existence of an additional linear contribution to the strain rate.

A vast body of experimental data exist proving that linear creep occurs in fine grained synthetic and fine grained or recrystallized natural salt by the mechanism of dissolution-precipitation creep (or pressure solution). Theoretical models for this process show a strong dependence on salt grain size[15, 16].

Conceptually, linear creep becomes more important at low deviatoric stresses, that prevail in the far field from salt caverns and when cavern pressure is allowed to increase closer to the lithostatic pressure in the post-production phase, which is the subject of this study.

In the Barradeel case (T = 378 K), BGR had neglected linear creep in their pre-production subsidence forecast; they only used n=5 power law creep (the 'official German standard', also mentioned in the KBB reports). BGR predicted 7 cm of subsidence in the deepest point after 40 years of production. In reality subsidence has reached almost 35 cm within some 10 years, 20 times faster than the BGR forecast[17].

In the Heiligerlee case (same Zechstein Z2 formation), operational differential stresses and temperature (T = 323 K) are lower than in the Barradeel case[17], so linear creep impact on subsidence is expected to be lower. However, it cannot *a priori* be assumed to be negligible, especially when looking at the long term behaviour of convergence and subsidence under differential stresses that probably are lower than during operational conditions, thereby enhancing the contribution from linear creep to the overall convergence and deformation process.

[15] Urai, J.L., Spiers, C.J., Zwart, H.J. & Lister, G.S. (1986b): Weakening of rock salt by water during long-term creep. Nature 324 (6097), pp. 554–557.
[16] Spiers, C.J., Schutjens, P.M.T.M., Brzesowsky, R.H., Peach, C.J., Liezenberg, J.L. & Zwart, H.J. (1990): Experimental determination of constitutive parameters governing creep of rocksalt by pressure solution. In: Knipe, R.J., Rutter, E.H. (Eds.), Deformation Mechanisms, Rheology and Tectonics. Geological Society, London, Special Publications, 54, pp. 215–227.
[17] Breunese, J.N., van Eijs, R.M.H.E., de Meer, S. & Kroon I.C. (2003): Observation and prediction of the relation between salt creep and land subsidence in solution mining—The Barradeel case, paper presented at SMRI Conference, Chester.

4.1.2 *Constitutive laws*

A vast amount of literature exists on, mostly empirical, constitutive laws for the microscopic behaviour of rock salt. We refer to Wallner et al. (2017)[18] for extensive overviews. At a high aggregation level, one may divide the proposed laws according to their specific strain rate dependence on differential stress according to:

1) power law behaviour only (stress exponent n usually between 3 and 6)
2) a combination of power law and linear (n=1).

The first group is usually referred to as the Norton-Hoff model type.
For the second case, two of the most important and applied constitutive model equations are:

The Ellis model [19]

$$\dot{\epsilon} = \dot{\epsilon}_{DC} + \dot{\epsilon}_{PS} = A_1^*.\ \sigma^n\ +\ A_2^*.\ \sigma$$

$$\text{with } A_1^* = A_1.\ \exp(-Q_1/RT)$$

$$A_2^* = A_2.\ \exp(-Q_2/RT)$$

$A_2 = 1 / 3\eta$ with η the temperature independent Maxwell viscosity

The Ellis model has 5 material property parameters: the set [A_1, Q_1, n] describes the power law creep rate and [A_2, Q_2] the linear creep rate, at temperature T.
The Ellis model is an additive parallel-mechanism formulation and is a general material law, not exclusive for rock salt. The Ellis model is fully consistent with state-of-the-art understanding of the physics of rock salt flow by dislocation creep (power law) and pressure solution creep (linear viscous law) (Spiers et al. 1990, Urai et al. 2008 [15] [16]).

The Lubby-2 model [20]

$$\dot{\epsilon} = (1/3h_M^*).\ \sigma.\ \exp(m.\sigma)$$

with Maxwell viscosity

$$h_M^* = h_{T0}^M.\ \exp(Q/RT).$$

The Lubby-2 model has (only) three parameters: [h_{T0}^M, Q, m].

For low deviatoric stresses, in a good approximation $\sigma.\ \exp(m.\sigma) = \sigma + m.\sigma^2$, and therefore at low deviatoric stresses the correspondence between the Ellis model and the Lubby-2 model is: $A_2^* = 1/3h_M^*$. In that sense, both model equations honour linear creep, be it in a mathematically somewhat different way.

---

[18] Wallner, M., Lux, K.-H., Minkley, W., & Hardy Jr, H.R. (Eds.). (2017): The mechanical behavior of salt – Understanding of THMC processes in salt: Proceedings of the 6th Conference on the Mechanical Behavior of Salt. Hannover, Germany, 22–25 May 2007. CRC Press
[19] Wang, L., Bérest, P. & Brouard, B. (2015). Mechanical behavior of salt caverns: Closed-form solutions vs numerical computations. *Rock Mech. Rock Eng.* 48: 2369-2382.
[20] Lux, K.-H. (1984): Gebirgsmechanischer Entwurf und Felderfahrungen im Salzkavernenbau (Ferdinand Enke Verlag, Stuttgart 1984)

4.2 Previous studies on caverns in the Winschoten salt dome

4.2.1 KBB Heiligerlee and Zuidwending

'Assumed creep response'
Enclosure 3 in the KBB-2015 report (Figure 4-1) shows a graphical representation of the 'assumed creep response' for the Heiligerlee caverns. The figure caption reads 'assumed creep response compared to Heiligerlee lab test results'. However, the figure does not contain any lab data.

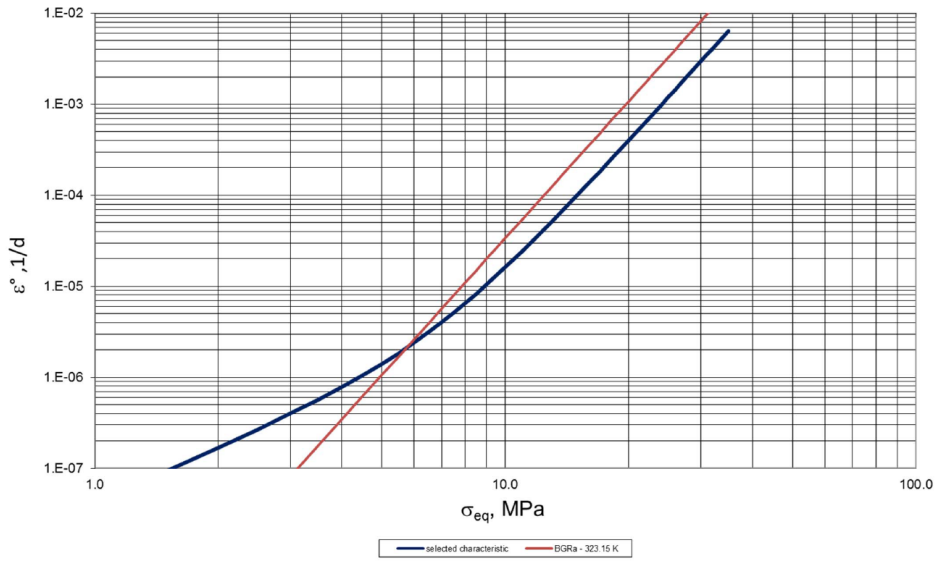

Figure 4-1: Enclosure 3 from KBB-2015 (Heiligerlee): Assumed creep response compared to Heiligerlee lab-test results.

In a similar KBB-2015 report on Zuidwending[10] also the 'assumed creep response' is shown in Enclosure 3 (Figure 4-2). In that figure, lab data are shown running down to 8 MPa deviatoric stress. We note that the drawn 'assumed creep response' curve does not fit to the lab data.

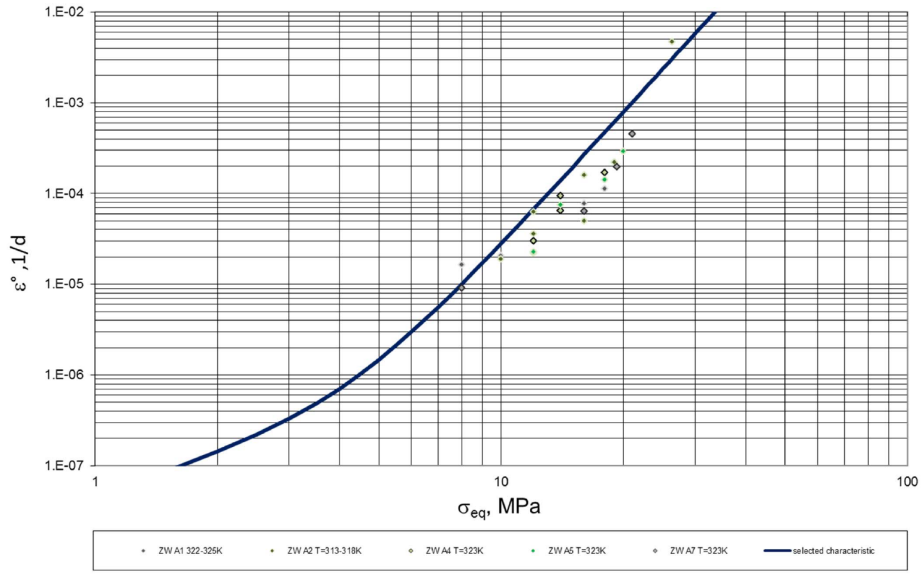

Figure 4-2 Enclosure 3 from KBB-2015 (Zuidwending): Assumed creep response compared to Zuidwending lab-test results.

Below 5 MPa, the 'Heiligerlee' and 'Zuidwending' assumed creep response curves are closely following each other, suggesting that KBB has assumed a similar - but unknown - function. Both cases point at a strain rate of around 5.10^{-8} (1/d) at 1 MPa, an indicator of the contribution of linear creep that KBB has assumed.

However, we remark that equation 3.3 from the KBB report describes the cavern convergence in terms of a power law only, i.e. does not honour linear creep at all.

TNO observes that:

- The 'assumed creep response' in the KBB reports is not explained and therefore could not be validated;
- There is a discrepancy between the graphical 'assumed creep response' curves (showing a tendency to honour linear creep at low deviatoric stresses) and the 'power law only' behaviour apparently actually used in the KBB modelling of cavern convergence, according to the text.

These observations have led us to look for further information on linear creep, relevant for the Heiligerlee case.

4.2.2 IfG Heiligerlee HL-K gas storage

In a 2016 report for Gasunie[11], IfG has applied the Lubby-2 creep law in a numerical assessment of the behaviour of the HL-K gas storage cavern. The model parameter values reported are:

$$\eta_{T0}^{M} = \ 0{,}188 \ \text{(MPa.d)}$$

$$m = \ 0{,}32$$

$$Q = \ 54 \ \text{(kJ/mol)} \ > \ \ Q/R = 6495 \ \ \text{(K)}$$

$$\eta_0^{M*} = 1{,}08 \cdot 10^8 \text{ (MPa.d)} \quad @ \quad T = 322$$

TNO observes that:

- The creep model used by IfG corresponds to a 6 times higher strain rate at 1 MPa than the value derived from the KBB 2015 study;
- The available lab data on salt creep do not run lower than 8 MPa deviatoric stress, still leaving quite some range of uncertainty as to the contribution of linear creep in the Heiligerlee situation.

These observations have inspired us to search for additional data, that might further constrain or at least underpin the range of uncertainty in the linear creep.

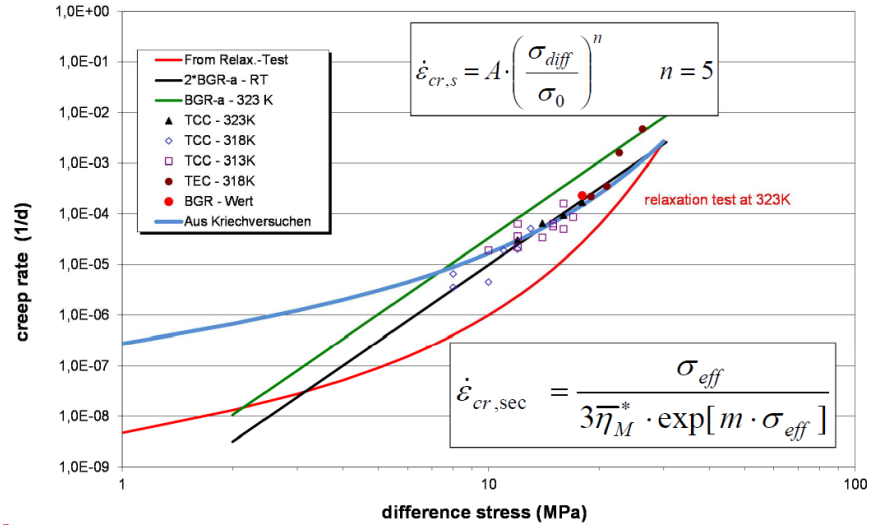

Figure 4-3: Creep rate versus differential stress in Heiligerlee HL-K cavern. Source IfG 2016 [11]

4.3 Model parameters

4.3.1 Linear creep data on the Zechstein Z2 formation in the Netherlands and Germany

Sources of information

We have focused our search for additional linear creep data to cases that pertain to the Zechstein Z2 formation, the same as in the Heiligerlee case. Moreover, we have geographically restricted our search to cases that are located at the southern edge of the Southern Permian Basin in the Netherlands and in Germany.

Three technically different sources of information have been found:

i. lab tests;
ii. tests executed in abandoned mines;
iii. results derived from field data on convergence and/ or subsidence.

Type i. and type ii. tests have in common, that they pertain to volumetrically small samples compared to the large salt body (order of km^3's) that geomechanically takes part in the cavern convergence and subsidence processes.

Type ii. tests typically have been executed to get to lower levels of deviatoric stress than is practically feasible in type i. lab tests. On the other hand, type i. tests can, and have been executed under quasi in-situ conditions regarding temperature and confinement pressure.

Type iii. tests are very rare: they are likely only to give information on linear creep, if creep rates are very high. The only case of this type known to us is the Barradeel solution salt mining from very deep caverns at 2.5 – 3 km depth and 100°C[17]. The results have been obtained from a FEM model by combining material balance data, sonar data and subsidence monitoring. In addition, lab data under simulated in-situ conditions from multiple caverns were available, some of which were long term tests extended down to 2 MPa deviatoric stress[21].
An important finding from these lab tests is, that the dependence of strain rate on deviatoric stress is not very sensitive to neither the depth in the cored Zechstein Z2 interval, nor the position of the cored well within de salt body in which solution mining takes place: the rheological behaviour appears to be more homogeneous than the large range of grain sizes in the core material suggests.

Summary of results

Table 4-1 summarizes our findings on linear creep within the searched area. These results are expressed in terms of the parameter A_2, which is temperature independent. We observe the following:

- The slow rate Barradeel lab tests show a 5 times higher linear creep rate at 1 MPa than the IfG report for Gasunie assumes, which can be explained by the impact of the higher in-situ temperature (378 versus 322 K);
- As for the parameter A_2, the range of outcomes from the Barradeel DIANA model favourably compares with the slow rate BAS-4 lab test data on samples from the same salt body; note that these lab data were not available, when the FEM was constructed and calibrated;
- The lab data from the Barradeel case (and also the Heiligerlee/ Zuidwending cases) indicate that the rheological behaviour appears to be more homogeneous than the large range (many orders of magnitude) of grain sizes as seen in the core material suggests;
- The slow rate mine test on samples from the Gorleben dome in Germany show a relatively high A_2 value compared to the other tests; this cannot be explained by temperature (281 K), which is lower than that in the other tests.

[21] IfG (2006). Rock mechanical investigations on rock salt from cavern well BAS4. Report for ESCO / Frisia Zout BV (17-10-2006)

Table 4-1: Summary of linear creep data related to research area.

	Year	σ_{min}	strain rate @ 1 MPa	temp.		A_2	
		(MPa)	(10^{-7} d^{-1})	(K)		(10^{-3} d^{-1})	
					low	mode	high
Assumed creep response							
KBB Heiligerlee	2015	8	0.5	322		0.57	
IfG Heiligerlee	2016	8	3	322		3.4	
Slow rate lab tests							
IfG BAS-1&2	2004	5		378	3.2		16
IfG BAS-4	2006	2	15	378		4.3	
BAS history match	*2010*	*n.a.*		*378*	*2.9*	*6.5*	*14.8*
BAS van Heekeren	*2009*	*n.a.*		*378*	*5*	*9*	*13*
Slow rate mine test							
Bérest et al. Gorleben	2019	0.2	10	281		44	

4.4 Model choices for this study

4.4.1 Constitutive model for salt creep

We have chosen to use the Ellis formulation of the salt creep model, because:

- The Ellis model has a more explicit physical representation of the linear creep mechanism;
- The Ellis model is readily available within the DIANA software (see Chapter 5).

We iterate, that the Lubby-2 model is also capable of introducing linear creep, be it in a different mathematical formulation. We do not feel that a choice for the Ellis model or for the Lubby-2 model is likely to significantly influence the results of this study: at this point, the fact that linear creep is honoured is more important than its exact formulation.

The full model chosen reads:

$$\dot{\varepsilon}_{axial} = A_1\, exp(-\frac{Q_1}{RT})(\frac{\Delta\sigma}{\alpha})^{n1} + A_2\, exp(-\frac{Q_2}{RT})(\frac{\Delta\sigma}{\alpha})^{n2}$$

where $\dot{\varepsilon}_{axial}$ is the vertical strain rate [1/s], $\Delta\sigma = \sigma_{axial} - \sigma_{radial}$ is the differential stress of a triaxial loading test [Pa]; A_1 and A_2 are the creep strain rate coefficients [1/s], Q_1 and Q_2 are the activation energies in [J/mol], R is the gas constant (8.314 J/K/mol), T is the ambient temperature [K], α is the reference stress [Pa]; n_1 and n_2 are the stress exponents for the non-linear creep (n_1 >1) and the linear creep (n_2=1), respectively; and α is the scaling factor for stress.

Four sets of values were used for the steady-state creep, referred to as: (i) the non-linear creep variant (NLC); (ii) the low linear creep variant (LLC); (iii) the medium linear creep variant (MLC) and (iv) the high linear creep variant (HLC). The variant

(i) is with the non-linear creep branch only, while the variants (ii, iii, iv) are a combination of the non-linear branch and the linear creep branch (Table 4-2).

Table 4-2: Salt creep property values for the various salt models used in simulations. A_1 and A_2 are the creep strain rate coefficients; Q_1 and Q_2 are the activation energies; R is the gas constant; n_1 and n_2 are the stress exponents; α is the stress scaling factor.

Salt creep model	A_1 [1/day]	n_1	Q_1/R [K]	A_2 [1/day]	n_2	Q_2/R [K]	α [MPa]
ZwdNLC Non-linear creep only	0.053	5	6495	-	-	-	1
ZwdNLLLC Non-linear + Low linear creep	0.053	5	6495	0.0005	1	3007	1
ZwdNLMLC Non-linear + Medium linear creep	0.053	5	6495	0.0030	1	3007	1
ZwdNLHLC Non-linear + High linear creep	0.053	5	6495	0.0150	1	3007	1

4.4.2 Parameter uncertainties

Linear creep

TNO has derived the uncertainty in the parameter A_2 from the data in Table 4.1, For practical reasons we have defined three cases for the modelling:

Low linear creep (LLC): A_2 = 0,0005 (1/day) cf. KBB 2015
Medium linear creep (MLC): A_2 = 0,003 (1/day) cf. IfG 2016
High linear creep (HLC): A_2 = 0,015 (1/day) cf. BAS-4 high value

Other parameters of the Ellis model

Of course, the other parameters of the Ellis model, in particular the power law creep term, have uncertainties as well. Since this part of the equation is much better constrained by lab data, we have chosen a deterministic best fit here, using data from Heiligerlee and Zuidwending.

Temperature dependence in the Ellis equation is described by the activation energies Q_1 and Q_2. When using lab data from the Heiligerlee / Zuidwending case (Figure 4-4), this temperature dependence is included in the model calibration as long as lab data have been acquired at in-situ temperatures (which is the case here).

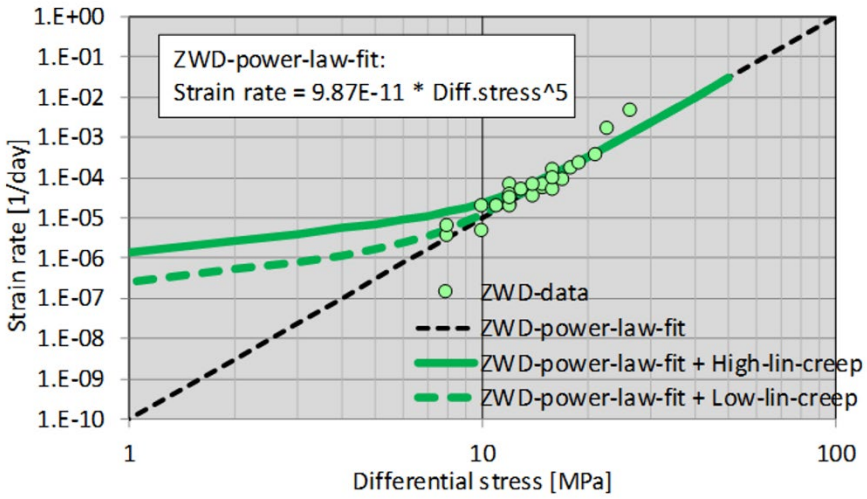

Figure 4-4: Creep models for the rock salt fitted to the Zuidwending experimental data (temperature range 313 – 323 K).

4.4.3 Limitations: stress threshold on linear creep

In the course of this project, TNO was advised by prof. C.J. Spiers from Utrecht University (pers. comm. 30-11-2020), that linear creep in rock salt is likely to be physically constrained at very low deviatoric stress levels. This argument is inspired by thermodynamics, which implies that at very low stresses surface energy effects outweigh the effects of stress in causing the fluid films that allow linear creep by pressure solution to heal, thus stopping the process. The concept is further supported by tectonic evidence for a threshold stress for salt flow and by the slow sinking rate of anhydrite rafts in salt bodies [22, 23, 15].

At the moment of writing of this report, laboratory research on this subject is ongoing. Prof. Spiers has indicated, that this threshold is likely to be in the range between 0.07 and 0.7 MPa for rock salt at depths relevant for the Heiligerlee situation (around 1 km), while deeper caverns at around 3 km may have a threshold at between 0.05 and 0.5 MPa (cf. the Barradeel case).

[22] Van Noort, R., Visser, H.J.M. & Spiers, C.J. (2008): Influence of grain boundary structure on dissolution controlled pressure solution and retarding effects of grain boundary healing. J. Geophys. Res. Solid Earth 113 (3), pp. 1–15.

[23] Desbois, G., Urai, J.L. & De Bresser, J.H.P. [2012]: Fluid distribution in grain boundaries of natural fine-grained rock salt deformed al low differential stress (Qom Kuh salt fountain, central Iran): Implicatios for rheology and transport properties, Journal of Structural Geology (2012) pp. 1-16.

4.4.4 Effects not covered by the Ellis equation

Prof. Spiers has also pointed at two other rock salt flow related phenomena, that are not included in the Ellis model formulation:

- *Dynamic recrystallization*, likely to occur at strains above 0.1 and typically leading to a creep acceleration by a factor 2[24, 25, 26].
- *Dilatancy*, occurring around a brine filled cavern during convergence, that may accelerate creep in the dilatant zone due to grain size reduction and brine penetration.

The effects of these phenomena will be discussed later in this report.

[24] Peach, C.J., Spiers, C.J. & Trimby, P.W. (2001): Effect of confining pressure on dilatation, recrystallization, and flow of rock salt at 150°C. J. Geophys. Res. 106 (B7), pp. 13,315-13,328.
[25] Ter Heege, J.H., De Bresser, J.H.P. & Spiers, C.J. (2005a): Rheological behaviour of synthetic rocksalt: The interplay between water, dynamic recrystallization and deformation mechanisms. J. Struct. Geol. 27 (6), pp. 948–963.
[26] Ter Heege, J.H., De Bresser, J.H.P. & Spiers, C.J. (2005b): Dynamic recrystallization of wet synthetic polycrystalline halite: Dependence of grain size distribution on flow stress, temperature and strain. Tectonophysics 396 (1–2), pp. 35–57.

5 Numerical single cavern modelling

This chapter describes the model setup, analysis setup, simulation scenarios and modelling results for a single cavern.

5.1 Model setup

The model setup comprises: (i) the simplified geometry of the overburden layers, of a salt dome and of a cavern, (ii) the constitutive models and material parameters' values for the differentiated model units, (iii) the in-situ state of stress and (iv) the various cavern pressure levels.

5.1.1 Model geometry

An axisymmetric geomechanical model of single cavern was constructed. The model is shown in Figure 5-1a. The model size is 3,000 m by 15,000 m (depth versus radius). The model boundaries were placed far away from the cavern to minimize the effects of boundaries on simulation results. The model layers were meshed using quadratic second-order eight-node quadrilateral ring elements for better solution accuracy. The displacement boundary conditions were imposed to constrain displacements in the direction normal to the outer model edge and the model base.

In the model the cavern is vertical, has an idealized cylindrical shape, a radius of 27 m and a volume of ca. 1 million m^3 (Figure 5-1b). The vertical axis of the cavern and the axis of rotational symmetry of the numerical model are aligned. The 450m-thick overburden at Heiligerlee comprises various stratigraphic and lithologic units: The North Sea clastic sediments, the Cretaceous chalk, the Rijnland sediments and the Germanic Trias sediments. In the numerical model, the geometry of the overburden is simplified and represented by two units: (i) the 200m-thick overburden 1 at the top and (ii) the 250m-thick overburden 2 at the bottom. The rock salt below the overburden lies in the depth range of 450 to 2900 m. There is a 100m-thick base rock layer below the salt. The salt layer can have "indefinite" lateral extent, when the radius of cylindrical salt dome is equal to the model length (15 km), or it can have a finite extent. We considered the cases with a salt dome radius of 500 m, 1000 m, 2000 m and 5000 m.

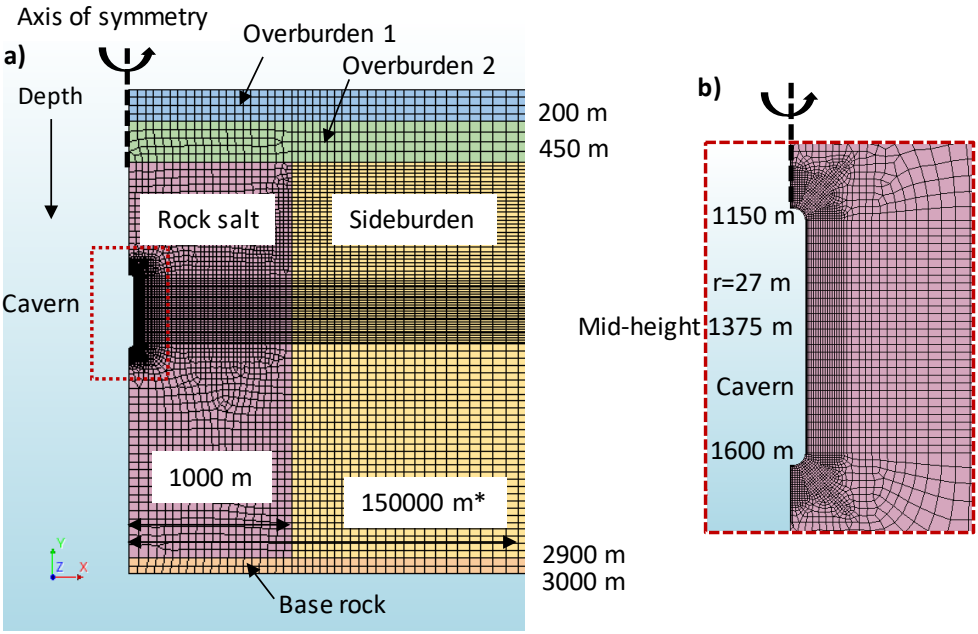

Figure 5-1: (a) Mesh for the axisymmetric model of single cavern and (b) enlarged part of the model around the cavern (side view). * - The model length (radius) is not to scale.

5.1.2 Materials and constitutive models

Material properties' values for the model units are listed in Table 5-1. The elastic properties of rock salt were measured on the core taken from the Zuidwending salt dome[27]. Physical, elastic and thermal properties' values for other units were adopted from the literature. All the layers, except the rock salt, were assumed to exhibit pure elastic behaviour. The layers have uniform properties.

Table 5-1: Material properties' values for the model units.

Layer	Density [kg/m^3]	Young's modulus [GPa]	Pois-son's coef.	Thermal expansion coef. [1/K]	Heat con-ductivity [J/(day m K)]	Heat capacity [J/(m^3 K)]]	Initial stress ratio, K_0***
Overburden 1	2050	1	0.25	3e-5	1.71e5	1.84e6	0.7
Overburden 2	2050	25	0.25	3e-5	1.71e5	1.84e6	0.7
Rock salt	2179	32	0.26	5e-5	4.28e5*	1.84e6**	1.0
Side-burden	2200	25	0.25	3e-5	1.71e5	1.84e6	0.7
Under-burden	2500	25	0.20	3e-5	1.71e5	1.84e6	0.7

* Heat conductivity=4.95 W/(m K); **Heat capacity=0.92 J/(g K); ***K_0=Ratio of minimum-to-maximum total stress.

[27] IfG (2007). Rock mechanical investigations on rock salt from the Zuidwending gas storage site. Report number 11/2007

5.1.3 *The material model for rock salt takes into account the steady-state creep driven by the differential stress. The constitutive model for the steady-state salt creep combines (i) a power-law branch for the non-linear creep and (ii) a linear branch for the pressure solution creep, as explained in Chapter 4. Stress and pressure analysis setup*

The main aspect considered is the creep of rock salt that requires nonlinear transient analysis. The analysis was setup as a phased (or staged) analysis. Two phases were defined: (i) phase 1 (PH1_Initialization) and (ii) phase 2 (PH2_CaveHL, Figure 5-2a).
In phase 1 the initial in-situ temperature and stress conditions were initialized. The cavern was not present in the model. In phase 2, the cavern (void) was introduced and different cases were simulated by varying the pressure levels of brine inside the cavern.

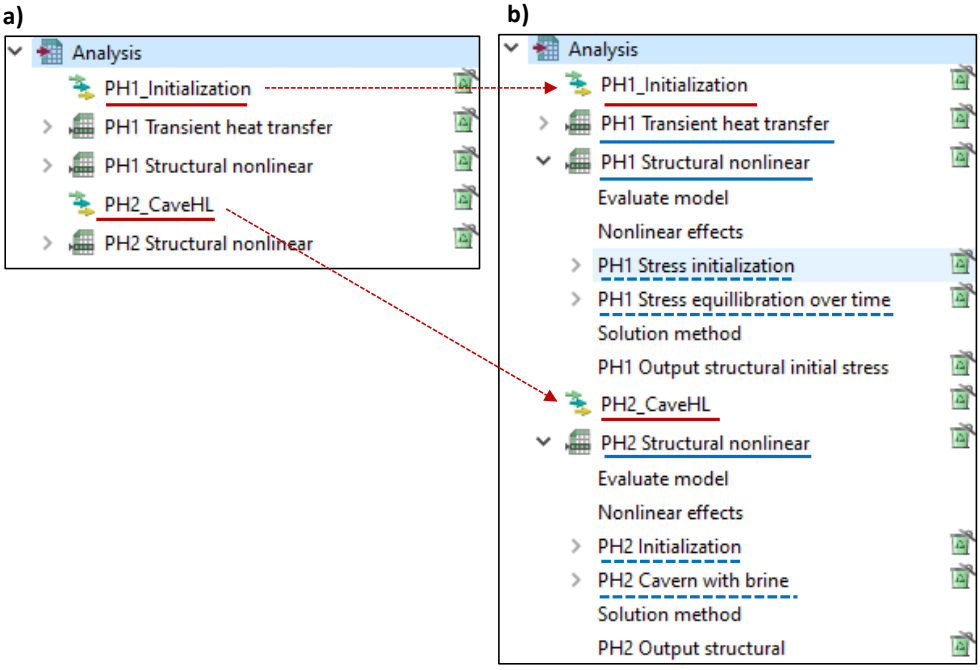

Figure 5-2: Analysis setup for the axi-symmetric single cavern model comprises (a) two phases (underlined red) and (b) several structural non-linear analysis steps (underlined blue).

Phase 1 comprises the following steps (Figure 5-2b):

- PH1 Transient heat transfer analysis - to initialize a depth-dependent temperature field equal to the in-situ rock temperature. Fixed or depth-dependent temperature was defined at model boundaries. The initial temperature field was calculated using the expression:

$$T = T_0 + K_T H$$

where T is the depth-dependent temperature [K], T_0 is the surface temperature [283 K] and K_T [0.025 K/m] is the average thermal gradient for rock salt. The resulting temperature field is shown in Figure 5-3. Temperature at the cavern mid-depth (1375 m) amounts to 317 K (45°C). Temperature variations over the cavern height is in the range of 312-323 K, i.e. 40-51°C. Note that the initial

temperature field remains unchanged during simulations, as the thermal effects of brine production were not considered in the analyses.

- PH1 Structural nonlinear - to apply the temperature field from the heat analysis and execute stress initialization and equilibration.
- PH1 Stress initialization - to initialize the in-situ stress in line with the K_0 total stress ratios per model unit listed in the last column of Table 5-1. Stress initialization with the different K_0-values per layer is straightforward for the model with layer-cake and horizontally continuous layers, i.e. in the model with "indefinite" salt extent. Stress initialization in the models with limited extent of salt dome is not straightforward. It requires a special procedure that leads to the correct initial isotropic stresses in salt (K_0=1) and non-isotropic stresses in the side burden (K_0=0.7). One option is to use the stress equilibration over time and the other is to reduce the shear modulus in salt during stress initialization. Both methods lead to the dissipation of differential stress in salt close to zero[28].
- PH1 Stress equilibration over time - to initialize the correct initial stresses in the models with limited salt extent. The gravity was applied and the stress in the creeping salt is allowed to equilibrate until the differential stress in salt becomes close to zero (below 0.001 MPa).

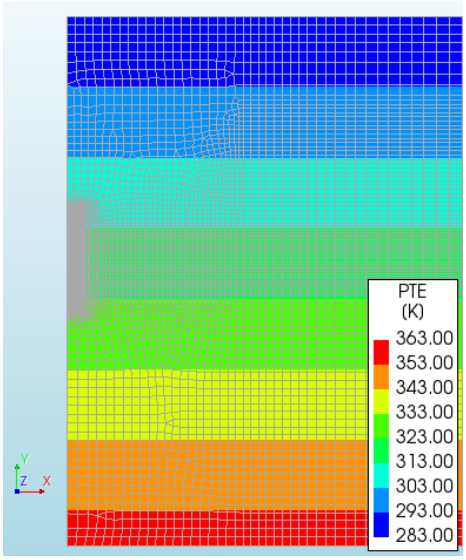

Figure 5-3: Initial depth-dependent temperature field in the model. For scale-reference see Figure 5-1a

Phase 2 comprises the following steps (Figure 5-2b):

- PH2 Structural nonlinear – to initialize the model with the cavern and simulate the different phases during cavern's lifetime.
- PH2 Initialization - to apply the in-situ stress from the previous phase 1 to the model and introduce the cavern initially supported by the lithostatic pressure inside the cavern.

[28] Orlic B. & Wassing B.B.T. (2013). A study of stress change and fault slip in producing gas reservoirs overlain by elastic and viscoelastic caprocks. Rock Mechanics and Rock Engineering. 46:421-435

- PH2 Cavern with brine – to simulate the different phases during the lifetime of cavern: the construction phase, the salt production phase and the phase of pressure control. The details of simulated loading scenarios are given in Table 5-2 and Figure 5-4.

In summary, we defined 20 scenarios by combining 1 loading scenario, 5 pressure levels during the phase of pressure control (Table 5-2) and 4 salt creep variants (Table 4-2).

Table 5-2: Loading scenarios simulated with the axisymmetric, single cavern model (P – pressure inside the cavern).

Phase of cavern's lifetime	Start/End [day]	Duration [day]	Duration [yr]	Cavern pressure
Cavern construction	0-1	1		Litho-P switched to halmostatic
Salt production	1-1800	1799	5.0	Halmostatic P
P-control, P-increase	1800-2100	300	0.8	P increase to 70,80,90,100% of litho-P
P-control, P-constant	2100-20000	18200	49.9	Constant elevated brine P

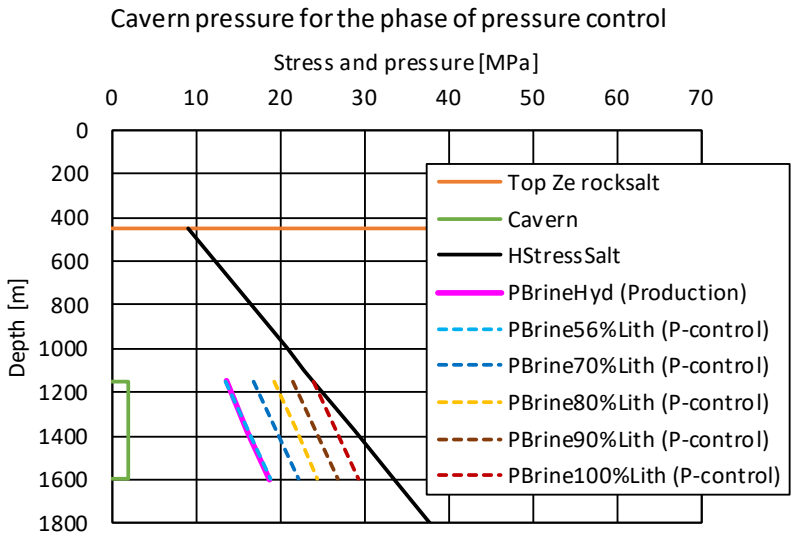

Figure 5-4: Brine pressure levels in the cavern considered in the simulation scenarios. PBrineHyd – halmostatic brine pressure equal to 56% of the lithostatic pressure in salt; PBrine70%Lith (P-control) - brine pressure increase to 70% of the litho-pressure during the phase of pressure control; etc. The reference depth for brine pressure levels is at the top of the cavern.

5.2 Results for a single cavern

The model was used to estimate the temporal evolution of cavern convergence and surface deformation. Here, we present the surface deformation profiles for the models with a salt dome radius of 1000 m (Figure 5-5), 500 m (Figure 5-6) and 2000 m (Figure 5-7). Each model is calculated with the four variants of salt creep law (Table 4-2). The pressure increase in the phase of pressure control amounts to 90% of lithostatic pressure (cap90). Figure 5-8 shows the effect of different pressure levels during the phase of pressure control on the evolution of the subsidence bowl for the model with a salt dome radius of 500 m.

Output items (displacements, strains and stresses) for estimation of cavern convergence rates are presented and analysed in conjunction with the analytical results in Section 6.2. The plots in Figure 5-5 – Figure 5-7 show the evolution of the subsidence bowl with time. The subsidence profiles depend on the radius of the salt dome and the salt creep law. Figure 5-8 shows that the subsidence profiles also depend on pressure levels during the phase of pressure control.

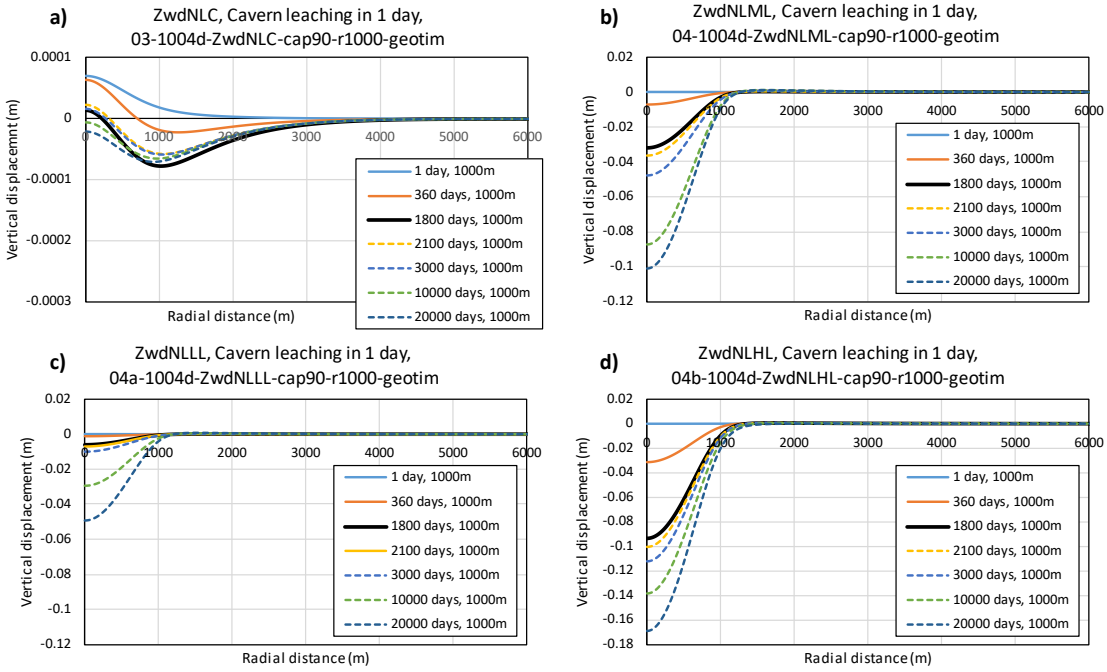

Figure 5-5: Evolution of surface deformation profiles (vertical displacement) above the salt cavern for a salt dome with radius of 1000 m. Cavern pressure increases to 90% of lithostatic pressure in the phase of pressure control. (a) Case with non-linear salt creep, (b) non-linear and medium linear creep, (c) non-linear and low linear creep, (d) non-linear and high linear creep.

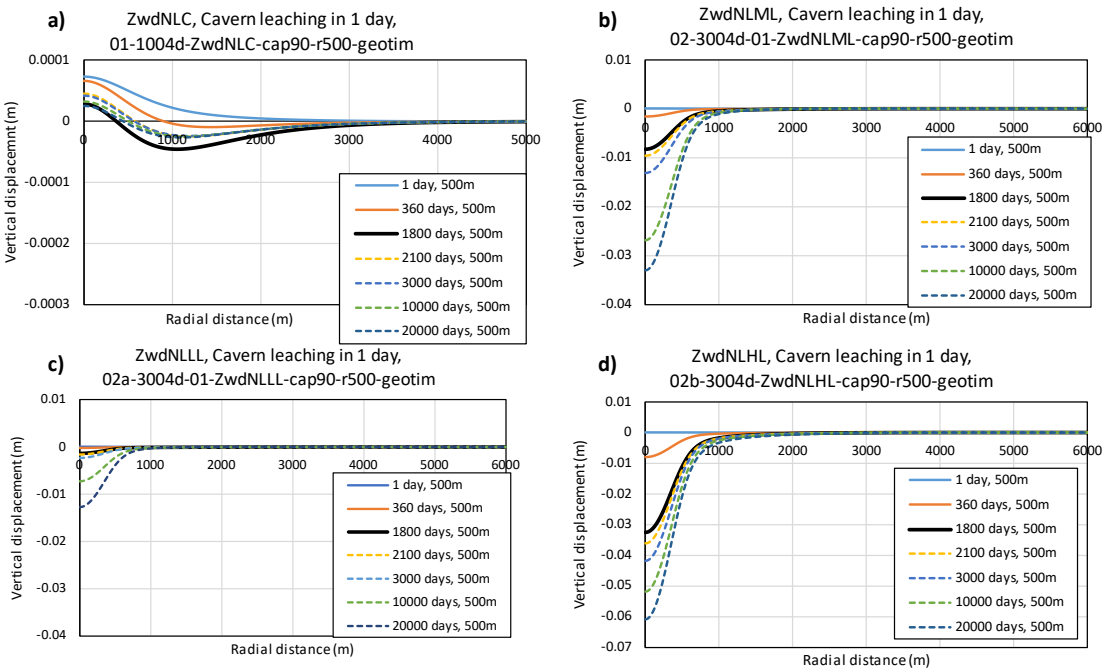

Figure 5-6: Evolution of surface deformation profiles (vertical displacement) above the salt cavern for a salt dome with radius of 500 m. Cavern pressure increases to 90% of lithostatic pressure in the phase of pressure control. (a) Case with non-linear salt creep, (b) non-linear and medium linear creep, (c) non-linear and low linear creep, (d) non-linear and high linear creep.

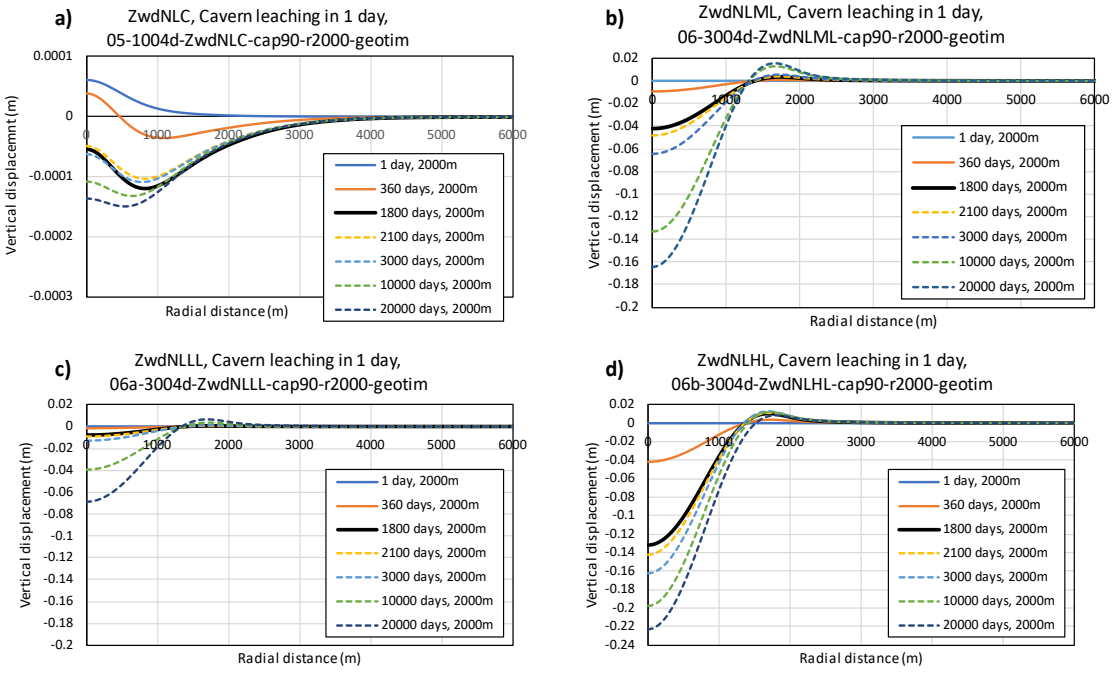

Figure 5-7: Evolution of surface deformation profiles (vertical displacement) above the salt cavern for a salt dome radius of 2000 m. Cavern pressure increases to 90% of lithostatic pressure in the phase of pressure control. (a) Case with non-linear salt creep, (b) non-linear and medium linear creep, (c) non-linear and low linear creep, (d) non-linear and high linear creep.

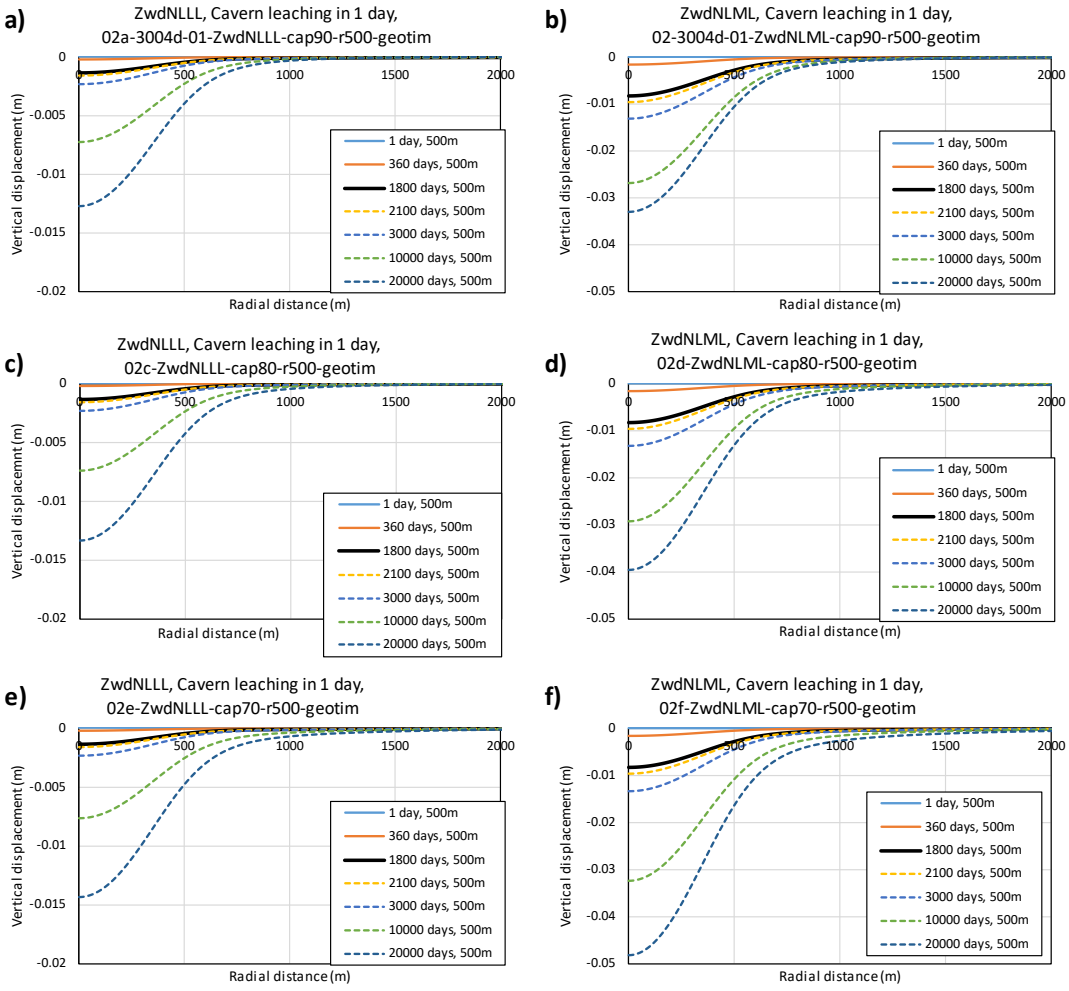

Figure 5-8: Evolution of surface deformation profiles (vertical displacement) above the salt cavern for a salt dome with radius of 500 m. Plots show effects of different pressure levels in the phase of pressure control. Left column of plots (a, c, e) - cases with the non-linear and low linear creep (NLLL). Right column of plots (b, d, f) – cases with the non-linear and medium linear creep (NLML). Cavern pressure increases to 90% (a, b), 80% (c, d) and 70% (e. f) of the lithostatic pressure in the phase of pressure control (cap90, cap80, cap70).

It is also possible to view the results from a different angle. Figure 5-9 shows the strong dependence of the subsidence bowl shape on the radius of the salt dome. The functions with 500 m and 1000 m dome radius give regular shapes with subsidence on top of the cavern, fading away when moving away from the centre. The case with extended salt layer gave uplift above the cavern and subsidence away from it. While this may be geomechanically reasonable[29], we deem it unrealistic for the domal structure here envisaged. The 5000-m dome gives an unrealistic pattern with an extended subsidence bowl and an uplifting bulge just inside the 5000 m extent from the centre. The 2000-m case shows the same behaviour to a lesser extent.

[29] Fokker, P.A. & Osinga, S. (2018, August). On the use of influence functions for subsidence evaluation. In 52nd US Rock Mechanics/Geomechanics Symposium. American Rock Mechanics Association.

In view of the actual geological situation for the Heiligerlee salt dome, in which a dome of a 1000 m radius is most appropriate, we choose the 500 m and 1000 m dome results for further investigation.

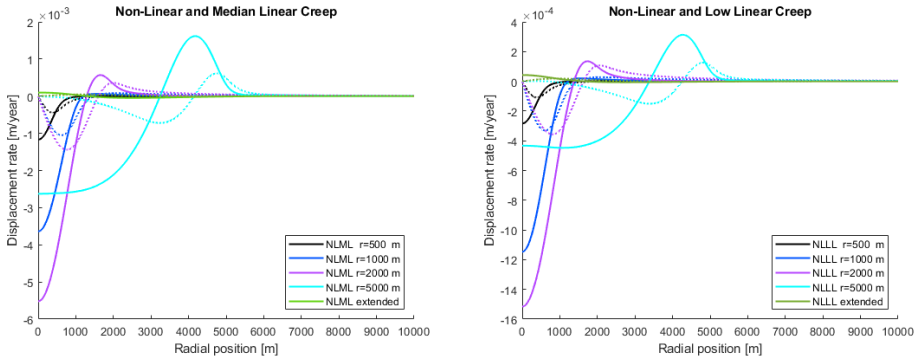

Figure 5-9: Yearly averaged subsidence resulting from salt cavern convergence between 3000 and 4000 days after start of the simulation, for the case with 1800 days halmostatic pressure, followed by a period with a pressure 90% of the virgin stress at the top of the cavity. The creep law with medium linear creep and low linear creep was employed. Colours indicate cases with different salt dome radii; solid curves indicate vertical movement and dashed curves indicate horizontal movement away from the centre of the subsidence bowl.

5.3 Derivation of influence functions

To make a prediction of subsidence during the production and post-production history of the salt cavern field in Heiligerlee, we make use of an influence function. Such an influence function can be used to estimate the cumulative effect of the development of the different caverns in the field. The influence function is defined as the scaled subsidence bowl during a unit time of squeeze (as an example, Figure 5-9 can be viewed as a collection of influence functions). For this we assume that the influence function for a certain choice of salt creep law and salt dome size is independent of the size of the cavern. However, it can be time dependent in two ways: the shape can change with time, and the magnitude as well.

To illustrate the time dependence of the shape, we plot in Figure 5-10 the scaled displacements for the NLML case. There is only some change in shape at the edge of the subsidence function. For the NLLL case the change in shape is even smaller (Figure 5-11). Thus, in a first investigation we used the shape of the influence function for the NLML and NLLL cases for the 500-m and 1000-m domes for all times.

An important correlation is the one between cavern squeeze volume and subsidence volume. For the cases with the extended salt layer, simulations show volume conservation after some equilibration time: all the cavern squeeze volume propagates to the surface subsidence bowl. This is not the case for the simulations with finite dome size. The non-zero rock compressibility facilitates expansion or compaction of the side burden, enabling the mismatch between the two volumes. Figure 5-12 shows how - for the NLML and NLLL cases - the different dome radii cause different evolutions of the subsidence bowl. For the 1000-m dome, the subsidence bowl volume slows down its increase rate only very slowly and the subsidence bowl volume is larger than the cavern squeeze volume. For the 500-m

dome, the volumes are much smaller; and the subsidence bowl volume is even smaller than the cavern squeeze volume.

In a first examination we used a single influence function to determine the effect of a converging salt cavern on the surface, with the magnitude development in terms of subsidence volume given as separate input with regard to the cavern squeeze volume. Figure 5-13 shows the increase rate of the cavern volume and of the subsidence bowl volume, for the NLML and the NLLL cases. We have corrected this later with the actual shape of the subsidence bowl at the corresponding times of the cavern evolution (cf. Ch. 8 and 9).

The starting assumption of this section was that the shape of the influence function is independent of the size of the cavern. An argument for this statement would be the spatial scalability of the displacements and the strain rates: scaling of the cavern radius with a factor will yield exactly the same results for the stresses at positions multiplied by that same factor. We will show in Chapter 6 that for infinitely extending layers, such scalability is indeed present. For the results in this chapter, however, the claim cannot be sustained, because there are a dome radius and a cavern height involved that do not change with the scaling. In addition, the salt dome size has a profound impact on the influence functions. We still argue, however, that the use of an influence function can be defended: the range of sizes of the actual caverns is limited (up to a factor 2 larger than the model cavern) and the functions for the most representative domes (500 m and 1000 m) are comparable in shape. Further, in Chapter 8 we will choose the best model based on a comparison with the observed subsidence rates.

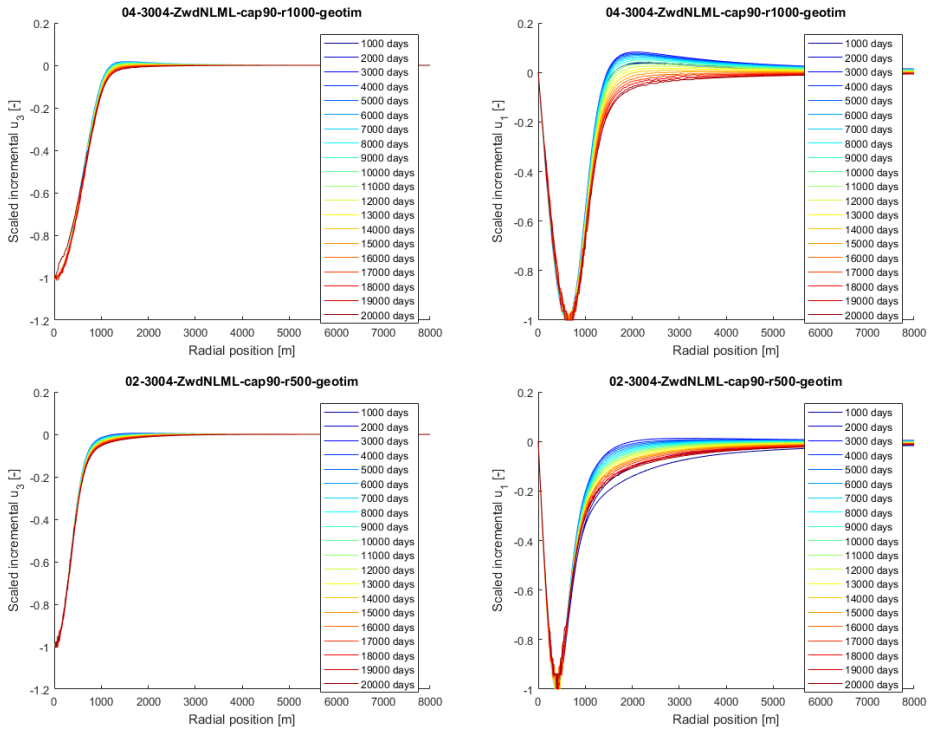

Figure 5-10: Incremental scaled vertical and horizontal displacements. Displacements are averaged over intervals of 1000 days and scaled to its maximum absolute value. Top row: 1000-m dome radius. Bottom row: 500-m dome radius.

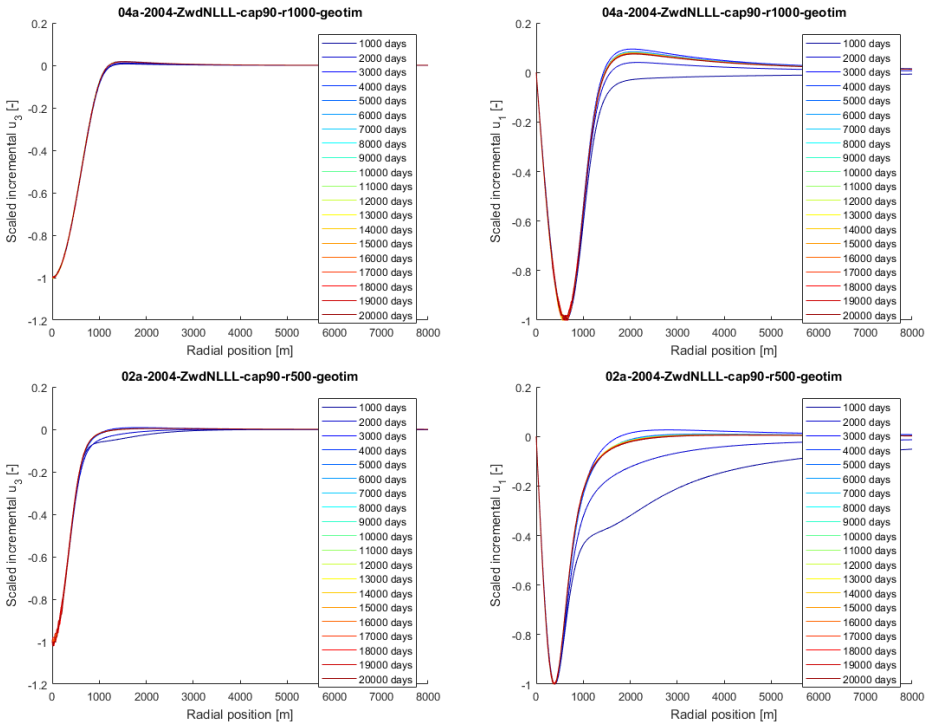

Figure 5-11: Incremental scaled vertical and horizontal displacements. Displacements are averaged over intervals of 1000 days and scaled to its maximum absolute value. After the 1800-days leaching period, there is no significant change in shape anymore. Top row: 1000-m dome radius. Bottom row: 500-m dome radius.

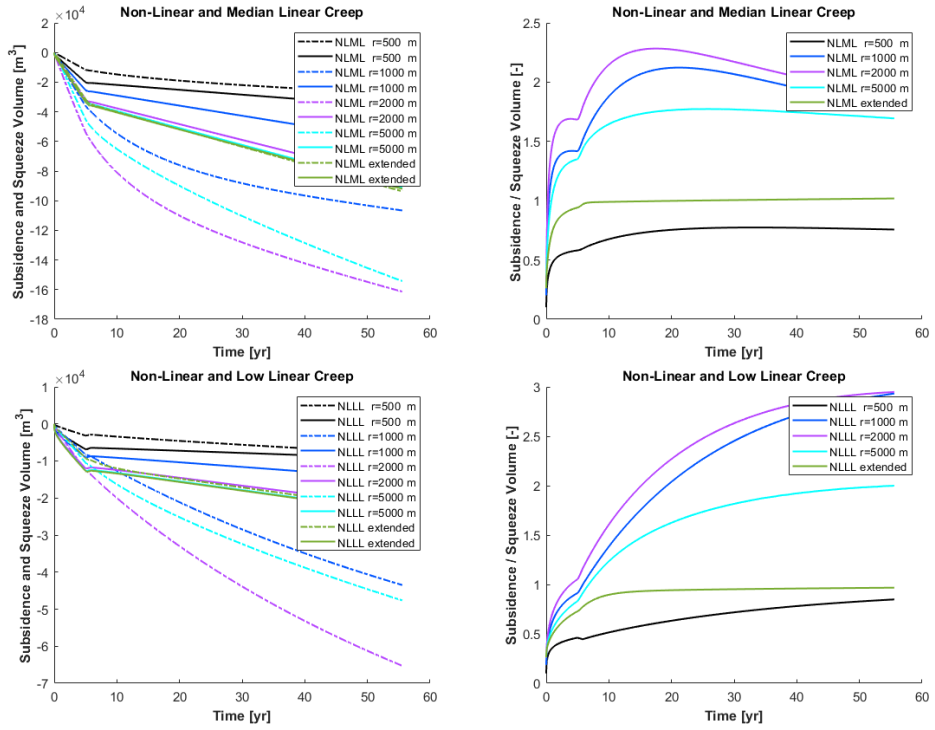

Figure 5-12: Volume evolution of cavern and subsidence bowl. Left: cavern volume loss (solid lines) and subsidence bowl volume (dashed lines) vs time for different dome radii. Right: Ratio of volume changes.

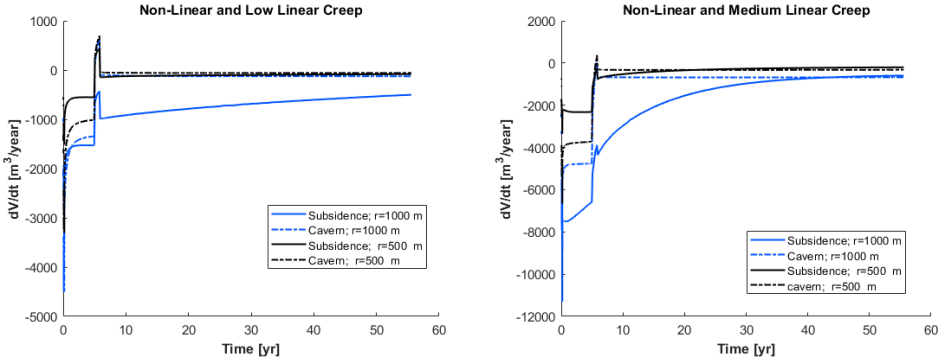

Figure 5-13: Increase rate of the salt cavern volume and of the subsidence bowl volume, for a cavern in a 1000-m and 500-m salt dome with NLLL properties (left) and NLML properties (right)

6 Analytical model for single cavern convergence

Here, we develop a new, analytical plane-strain approach for single cavern convergence (conform approach in Chapter 1 and 3). This new model is relevant for the salt squeeze behaviour. However, it is not relevant for the subsidence, because all displacements are strictly horizontal. For the subsidence we thus rely on influence functions derived from numerical simulations as outlined in Chapter 5.

The plane-strain convergence model represents a cavern in which the height is much larger than the horizontal dimensions of interest; therefore, the results are applicable at distances from the cavern that are smaller than its height.

6.1 Theoretical treatment

The following solves the convergence rate for a salt cavern in which the pressure is smaller than the lithostatic stress. We follow an approach similar to the one by Cornet et al (2017)[30], but employ the Ellis model rather than his Carreau model. The Ellis model is based on the physics principle of superposition of linear pressure-solution creep and power-law dislocation creep[31]. We use the more precise formulation of Wang et al (2015)[19].

We consider plane-strain conditions. The total stress is denoted as having a radial, tangential and vertical component. Because of cylindrical symmetry, these are principal stresses:

$$\boldsymbol{\sigma} = \begin{pmatrix} \sigma_{rr} & 0 & 0 \\ 0 & \sigma_{\theta\theta} & 0 \\ 0 & 0 & \sigma_{zz} \end{pmatrix} \qquad 1$$

We employ the negative compressive stress formulation. Then, we define the mean stress p, the deviatoric stress tensor $\boldsymbol{s}$ and its second invariant J_2, and, for later convenience, the maximum horizontal shear stress τ. q corresponds to the Von Mises stress σ_{VM}. We also define the Von Mises strain rate $\dot{\epsilon}_{VM}$.

$$\begin{aligned}
&p = -\tfrac{1}{3}(\sigma_{rr} + \sigma_{\theta\theta} + \sigma_{zz}) \\
&s_{ij} = \sigma_{ij} + p\delta_{ij} \\
&\mathbf{s} = \begin{pmatrix} \sigma_{rr} + p & 0 & 0 \\ 0 & \sigma_{\theta\theta} + p & 0 \\ 0 & 0 & \sigma_{zz} + p \end{pmatrix} \\
&J_2 = \tfrac{1}{2} s_{ij} s_{ji} = \tfrac{1}{6}\{(\sigma_{rr} - \sigma_{\theta\theta})^2 + (\sigma_{\theta\theta} - \sigma_{zz})^2 + (\sigma_{zz} - \sigma_{rr})^2\} \qquad 2 \\
&\sigma_{VM} = q = \sqrt{3J_2} = \sqrt{\tfrac{1}{2}\{(\sigma_{rr} - \sigma_{\theta\theta})^2 + (\sigma_{\theta\theta} - \sigma_{zz})^2 + (\sigma_{zz} - \sigma_{rr})^2\}} \\
&\tau = \tfrac{1}{2}(\sigma_{rr} - \sigma_{\theta\theta}) \\
&\dot{\epsilon}_{VM} = \sqrt{\tfrac{1}{2}\{(\dot{\epsilon}_{rr} - \dot{\epsilon}_{\theta\theta})^2 + (\dot{\epsilon}_{\theta\theta} - \dot{\epsilon}_{zz})^2 + (\dot{\epsilon}_{zz} - \dot{\epsilon}_{rr})^2\}}
\end{aligned}$$

[30] Cornet, J., Dabrowski, M. & Schmid, D.W. (2017). Long-term cavity closure in non-linear rocks. *Geophysical Journal International*, *210*(2), 1231-1243.
[31] Van Keken, P.E., Spiers, C.J., Van den Berg, A.P. & Muyzert, E.J. (1993). The effective viscosity of rocksalt: implementation of steady-state creep laws in numerical models of salt diapirism. *Tectonophysics*, *225*(4), 457-476.

The plane-strain condition implies that the strain rate is only dependent on the radial velocity v_r and the vertical strain rate is zero.

$$\begin{aligned}\dot{\epsilon}_{rr} &= \frac{\partial v_r}{\partial r} \\ \dot{\epsilon}_{\theta\theta} &= \frac{v_r}{r} \\ \dot{\epsilon}_{zz} &= 0\end{aligned} \tag{3}$$

Incompressible flow requires

$$\dot{\epsilon}_{rr} + \dot{\epsilon}_{\theta\theta} = 0 \tag{4}$$

This allows to solve for the velocity and the strains as

$$\begin{aligned}v_r &= v_R \frac{R}{r} \\ \dot{\epsilon}_{rr} &= -\dot{\epsilon}_{\theta\theta} = -v_R \frac{R}{r^2} \\ \frac{\partial \dot{\epsilon}_{rr}}{\partial r} &= 2v_R \frac{R}{r^3} = -\frac{2}{r}\dot{\epsilon}_{rr} \\ \dot{\epsilon}_{VM} &= \sqrt{3}|\dot{\epsilon}_{rr}|\end{aligned} \tag{5}$$

Here, v_R is a constant. It signifies the velocity at the cavern boundary where $r = R$.

We define the apparent viscosity through the relation between deviatoric stress and strain rate in equilibrated conditions. We will employ a model in which the apparent viscosity depends only on the second stress invariant, or q.

$$\dot{\epsilon}_{ij} = \frac{1}{\mu_{app}} s_{ij} \tag{6}$$

Inserting this into the incompressible-flow relationship (Eq. 4) yields $\dot{\epsilon}_{rr} + \dot{\epsilon}_{\theta\theta} = \frac{1}{\mu_{app}}(s_{rr} + s_{\theta\theta}) = \frac{1}{3\mu_{app}}(\sigma_{rr} - 2\sigma_{zz} + \sigma_{\theta\theta}) = 0$, which relates the vertical to the horizontal stresses and simplifies the stress invariants:

$$\begin{aligned}\sigma_{zz} &= \tfrac{1}{2}(\sigma_{rr} + \sigma_{\theta\theta}) \\ J_2 &= \tfrac{1}{4}(\sigma_{rr} - \sigma_{\theta\theta})^2 = \tau^2 \\ p &= -\tfrac{1}{2}(\sigma_{rr} + \sigma_{\theta\theta}) \\ \tau &= \sigma_r + p \\ q &= \tfrac{1}{2}\sqrt{3}|\sigma_{rr} - \sigma_{\theta\theta}| = \sqrt{3}|\tau| \\ \mu_{app} &= \frac{\tau}{\dot{\epsilon}_{rr}}\end{aligned} \tag{7}$$

Because of quasi-steady conditions, the equilibrium equation must be obeyed:

$$\frac{\partial \sigma_{rr}}{\partial r} + \frac{\sigma_{rr} - \sigma_{\theta\theta}}{r} = 0 \tag{8}$$

Substituting the expressions in terms of τ and p (Eqs. 2 and 7), the definition for the apparent viscosity (Eq. 6), and the expression for $\dot{\epsilon}_{rr}$ (Eq. 5) we obtain

$$\begin{aligned} -\frac{\partial p}{\partial r}+\frac{\partial \tau}{\partial r}+\frac{2\tau}{r}=0 \\ -\frac{\partial p}{\partial r}+\frac{\partial \mu_{app}}{\partial r}\dot{\epsilon}_{rr}=0 \end{aligned} \quad 9$$

This expression is still independent from the definition of the apparent viscosity.

In the Ellis model[31], the displacement rate is taken to be the sum of a power law term and a linear term with respect to the deviatoric stress. Physically, this combination represents dislocation creep and solution-precipitation creep (pressure solution), respectively. This sum defines the apparent viscosity (using the notation of Urai et al, 2008[32]):

$$\begin{aligned} &\dot{\epsilon}_{rr}=\dot{\epsilon}_{DC}+\dot{\epsilon}_{PS}=Ae^{-\frac{Q_{DC}}{RT}}\cdot(2\tau)^n+\frac{B}{TD^m}e^{-\frac{Q_{PS}}{RT}}\cdot 2\tau=\alpha\tau^n+\beta\tau \\ &\mu_{app}=\frac{\tau}{\dot{\epsilon}_{rr}}=\frac{|\tau|}{\dot{\epsilon}_{VM}}=\frac{1}{\beta}\cdot\frac{\tau}{\tau+\gamma\cdot\tau^n}=\frac{1}{\beta+\alpha\cdot\tau^{n-1}} \\ &\gamma=\frac{\alpha}{\beta} \end{aligned} \quad 10$$

As a result, we calculate the second term in the rewritten equilibrium equation (Eq. 9), and this term appears to have an analytic form:

$$\begin{aligned} \frac{\partial \mu_{app}}{\partial r}\dot{\epsilon}_{rr}&=-\mu_{app}^2\frac{\partial}{\partial r}(\alpha\tau^{n-1})\cdot\dot{\epsilon}_{rr}=(1-n)\mu_{app}^2\alpha\tau^{n-2}\frac{\partial\tau}{\partial r}\cdot\frac{\tau}{\mu_{app}} \\ &=(1-n)\mu_{app}\alpha\tau^{n-1}\frac{\partial\tau}{\partial r}=(1-n)\frac{\gamma\cdot\tau^n}{\gamma\cdot\tau^n+\tau}\frac{\partial\tau}{\partial r} \\ &=(1-n)\cdot\frac{\partial}{\partial r}\int\frac{\gamma\cdot\tau^n}{\gamma\cdot\tau^n+\tau}d\tau \\ &=(1-n) \\ &\cdot\frac{\partial}{\partial r}\left\{\tau-\tau\cdot\ {}_2F_1\left(1,\frac{1}{n-1};\frac{n}{n-1};-\gamma\cdot\tau^{n-1}\right)+constant\right\} \end{aligned} \quad 11$$

The last step involves an integration, in which the symbol ${}_2F_1$ denotes the hypergeometrical function.

The formulation of the second term in the equilibrium equation (Eq. 9) as a derivative with regard to the radial coordinate enables its integration. Incorporating the boundary condition that at infinity $p=\bar{p}$ and $\tau=0$, and using the definition of the stresses in a second step, we obtain:

$$\begin{aligned} p&=\bar{p}+(1-n)\cdot\tau\cdot\left\{1-\ {}_2F_1\left(1,\frac{1}{n-1};\frac{n}{n-1};-\gamma\cdot\tau^{n-1}\right)\right\} \\ \sigma_r&=-p+\tau=-\bar{p}+\tau\cdot\left\{n-(n-1)\cdot\ {}_2F_1\left(1,\frac{1}{n-1};\frac{n}{n-1};-\gamma\cdot\tau^{n-1}\right)\right\} \end{aligned} \quad 12$$

This equation implies an analytical relationship between the mean stress p and the shear stress τ.

[32] Urai, J.L., Schléder, Z., Spiers, C.J., & Kukla, P.A. (2008). Flow and transport properties of salt rocks. *Dynamics of complex intracontinental basins: The central European basin system*, 277-290.

At the inner boundary, we should have $\sigma_r = -p_w$. Therefore, we have

$$\bar{p} - p_w = \tau_R \cdot \left\{ n - (n-1) \cdot \ {}_2F_1 \left(1, \frac{1}{n-1}; \frac{n}{n-1}; -\gamma \cdot \tau_R^{n-1} \right) \right\} \quad 13$$

This equation must be solved for τ_R, which is the deviatoric stress at the rim. That solution is independent of the cavern radius R. Therefore, the solution is not explicitly dependent on the cavern size and can be scaled. The velocity at the rim is calculated as

$$v_R = -R\dot{\epsilon}_R = -R\frac{\tau_R}{\mu_{app}} = -R(\alpha\tau_R^n + \beta\tau_R) \quad 14$$

The convergence rate follows immediately:

$$\frac{1}{V}\frac{dV}{dt} = \frac{2}{R}\frac{dR}{dt} = \frac{2}{R}\, v_R = -2(\alpha\tau_R^n + \beta\tau_R) \quad 15$$

And the velocity in the full domain, and the strains result as

$$\begin{aligned} v_r &= v_R\frac{R}{r} = -\frac{R^2}{r}\frac{\tau_R}{\mu_{app}} = -\frac{R^2}{r}(\alpha\tau_R^n + \beta\tau_R) \\ \dot{\epsilon}_{rr} &= -\dot{\epsilon}_{\theta\theta} = \frac{R^2}{r^2}(\alpha\tau_R^n + \beta\tau_R) \end{aligned} \quad 16$$

The stresses must be determined by inverting the stress-strain constitutive relationship (Eq. 10).

6.2 Comparison with numerical results

As a benchmark the analytical results have been compared with the DIANA model calculations of Chapter 5.

First, we need to associate the input parameters for DIANA with the input parameters for the analytical correlations. The DIANA parameters are based on the double-creep law defined in terms of the Von-Mises strain rates and stress:

$$\dot{\epsilon}_{VM} = A_1 \exp\left[-\frac{Q_1}{RT}\right] q^n + A_2 \exp\left[-\frac{Q_2}{RT}\right] q \quad 17$$

Because $\dot{\epsilon}_{VM} = \sqrt{3}|\dot{\epsilon}_{rr}|$, $q = \sqrt{3}|\tau|$ and we defined our Ellis model as $\dot{\epsilon}_{rr} = \alpha\tau^n + \beta\tau$, we have

$$\begin{aligned} \alpha &= A_1 \exp\left[-\frac{Q_1}{RT}\right]\sqrt{3}^{n-1} \\ \beta &= A_2 \exp\left[-\frac{Q_2}{RT}\right] \end{aligned} \quad 18$$

The numbers used in the calibration are represented in Table 6-1.

Table 6-1: Model parameters

Model	NLC	NLLL	NLML	NLHL
T [K]	317			
A_1 [$\mathrm{Pa}^{-n}\mathrm{s}^{-1}$]	6.13426*10^{-37}			
$\frac{Q_1}{R}$ [K]	6495			
n [−]	5			
A_2 [$\mathrm{Pa}^{-1}\mathrm{s}^{-1}$]	0	1.73611*10^{-13}	3.47222*10^{-14}	5.78704*10^{-15}
$\frac{Q_2}{R}$ [K]	3007			
α [$\mathrm{Pa}^{-n}\mathrm{s}^{-1}$]	6.977*10^{-45}			
β [$\mathrm{Pa}^{-1}\mathrm{s}^{-1}$]	0	4.3936*10^{-19}	2.6362*10^{-18}	1.1318*10^{-17}

Figure 6-1 and Figure 6-2 represent results of the stress and strain rate fields at the centre depth of the cavern versus distance. For the case with only non-linear creep (Figure 6-1) agreement is poor due to the very slow, geometrically induced creep (see also Wang et al, 2015). For the Ellis model with intermediate linear creep parameters agreement between numerical and analytical results is excellent (Figure 6-2).

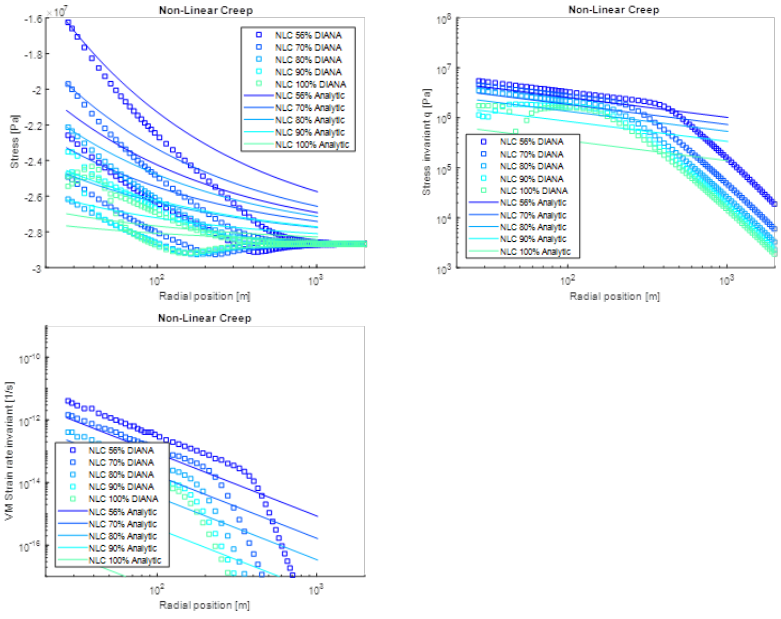

Figure 6-1: Benchmark results for the case with non-linear creep only. Figures denote the horizontal stresses (radial and tangential); deviatoric stress invariant and Von Mises strain rate invariant. Different colours denote the different cases for cavern pressure. The agreement is poor due to the very slow, geometrically induced creep.

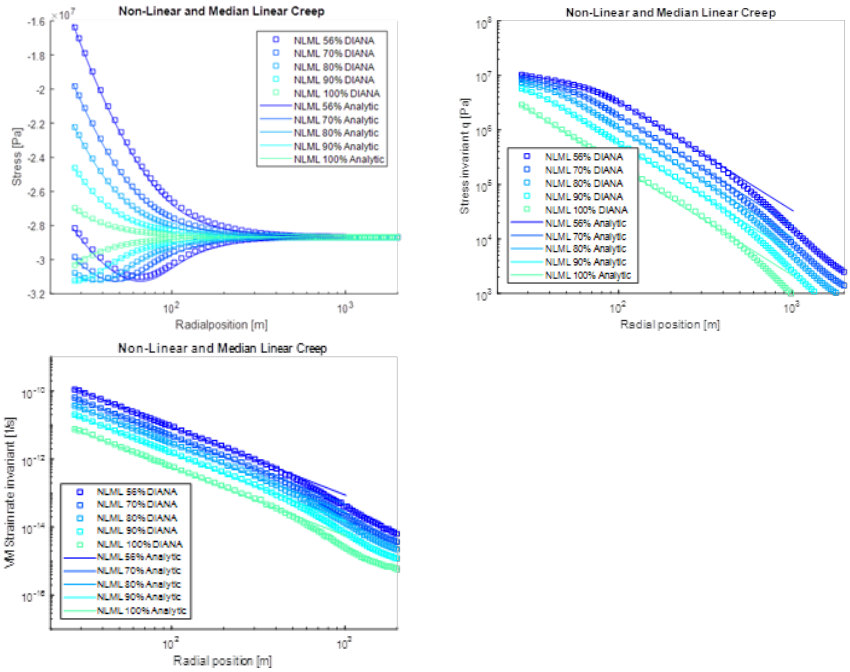

Figure 6-2: Benchmark results for case with non-linear and medium linear creep with the same coding as in Figure 1. The agreement is good for distances smaller than 500 m.

The numerical simulations map a cavern in 3D, meaning that the stress and strain rate curves depend on the height position in the cavern. Thus, part of the mismatch between analytic and numerical results is explained by the fact that there are also vertical rates in the numerical results. These partly compensate the horizontal ones, so the strain rate invariants agree (Figure 6-2 and Figure 6-3).

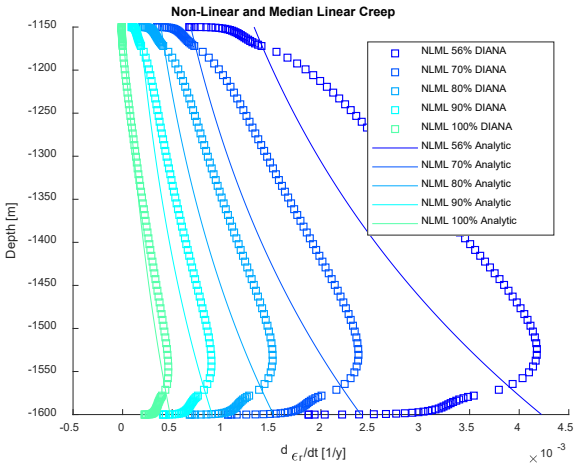

Figure 6-3: Horizontal strain rates versus depth for the Ellis model with intermediate linear creep parameters.

The analytic results give the volumetric squeeze rate for the prevailing input parameters. These can be calculated as a function of the depth, since both the temperature and the pressure difference are depth-dependent. Next, we integrated the results over the height of the cavern in the numerical simulations and derived in

this way the total volumetric squeeze rate. A comparison with the numerical results is provided in Table 6-2. Again, the results for the power law model do not agree, but the 80% agreement for the other models is good (given the plane-strain assumption).

Another important outcome of this analysis is the range of outcomes, which spans two orders of magnitude. In fact, the numbers depend on both the cavern pressure and the linear-creep parameters: within the three creep models, an increase of the pressure from 56% to 90% of the stress results in a 4 – 8-fold reduction in squeeze rate. Thus, only if the creep parameters are constrained better, we can provide a trustworthy pressure guideline for cavern abandonment.

The results presented in this chapter turn out to have limited value for the final questions addressed. In the first place, they do not provide subsidence estimates. In the second place, the numerical results with the finite dome sizes presented in the previous chapter show a large variability resulting from its actual value. The insight, however, corroborates the previous findings: linear creep profoundly influences the cavern squeeze rates and knowledge of its impact is crucial for making reliable estimates for the magnitude of its effect. This is important in view of the limited attention that is given to these issues in the current body of literature on the subject.

Table 6-2 Comparison of analytical and numerical squeeze rates for the benchmark cases. The cavern pressure is given as its ratio to the virgin lithostatic stress at the cavern top. Squeeze rates are given as percentage of the total cavern volume per year. The Ellis model employs the combination of non-linear creep and linear creep – results for 3 levels of the latter are represented here.

Model	**Pressure**	**Numerical (%)**	**Analytical (%)**
Power law	0.56 (halmostatic)	0.081	0.0063
	0.70	0.016	0.0015
	0.80	0.0033	0.00039
	0.90	0.0013	0.00007
	1.00	-0.0015	0.000005
Ellis / low-magnitude linear creep parameters	0.56 (halmostatic)	0.19	0.16
	0.70		0.075
	0.80		0.041
	0.90	0.019	0.020
	1.00		0.007
Ellis / medium-magnitude linear creep parameters	0.56 (halmostatic)	0.63	0.50
	0.70	0.35	0.28
	0.80	0.21	0.17
	0.90	0.11	0.093
	1.00	0.048	0.041
Ellis / high-magnitude linear creep parameters	0.56 (halmostatic)	2.1	1.7
	0.70		1.1
	0.80		0.70
	0.90	0.53	0.42
	1.00		0.20

7 Numerical multi-cavern model

The following sections describe model setup, analysis setup, simulation scenarios and results. The geomechanical model of multiple caverns comprises: (i) six caverns with an idealized circular cross-section embedded in the rock salt (ii) the constitutive model and material parameters' values for the rock salt, (iii) the in-situ state of stress and (iv) various pressure levels in caverns.
The loading scenarios used here were the same as for the axisymmetric benchmark model (cf. Chapter 5). Simulation of the production history at Heiligerlee was beyond the scope of this study.

7.1 Model setup

A geomechanical plane-strain model with six caverns ranging in size from 25 m to 58 m was constructed. The model size is 4,000 m by 4,000 m (Figure 7-1). It was meshed using quadratic, second-order quadrilateral and triangular, general plane strain elements for better solution accuracy. To constrain displacements in the direction normal to the edges the displacement boundary conditions were prescribed at the model edges (no material balance). The constitutive models and material parameters' values for the rock salt were the same as in simulations with the axi-symmetric benchmark model (Paragraph 5.1.1).

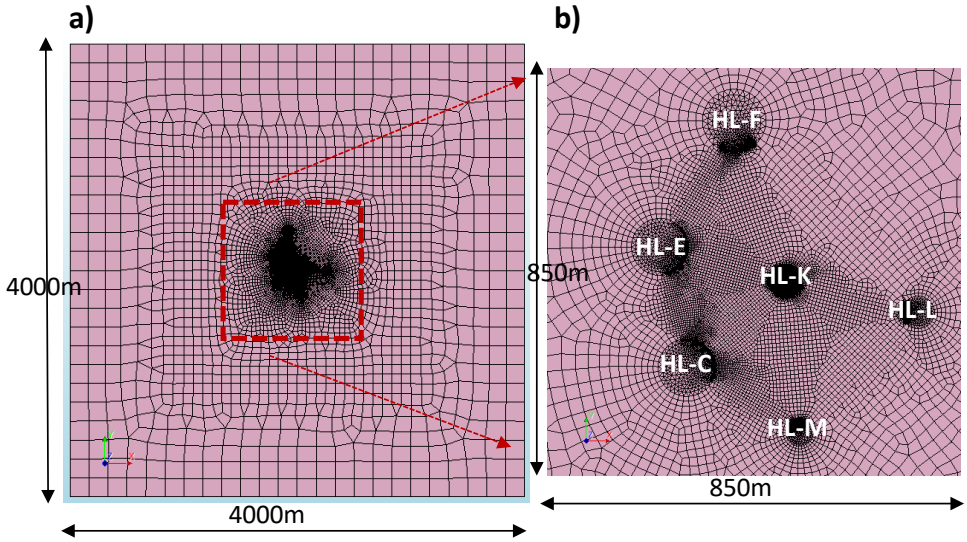

Figure 7-1: (a) Plane strain model of multiple caverns at Heiligerlee and (b) enlarged central part of the model with six caverns (top view). The plane strain model is a horizontal slice at half depth of the benchmark cavern (1375 m).

7.2 Analysis setup

The main aspect considered is whether the existence of a nearby cavern changes the behaviour of the other caverns. A phased analysis was setup with two phases: (i) phase 1 (PH1 Full model) and (ii) phase 2 (PH2 HLF Lifetime, Figure 7-2).
In phase 1 the initial in-situ temperature and stress conditions were initialized without the presence of any caverns. In phase 2, one cavern or multiple caverns

were introduced and different cases were simulated by varying the pressure levels of brine inside the cavern.

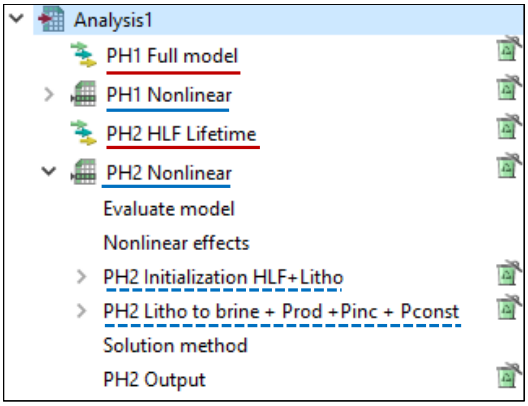

Figure 7-2: (a) Analysis setup for the plane strain model comprises (a) two phases (underlined red) and (b) the structural non-linear analysis in each phase (underlined blue).

Phase 1 comprises one step (Figure 7-2):

- PH1 Nonlinear analysis - to initialize the uniform temperature field equal to the in-situ rock temperature of 317 K (45°C) at a depth of 1375 m. The initial temperature field remains unchanged during simulations as the thermal effects of brine production were not considered. The in-situ stress in the rock salt was also initialized. We used the prestress option to ensure initialization of isotropic stresses in salt, without any shear stress.

Phase 2 comprises the following steps (Figure 7-2b):

- PH2 Nonlinear – to initialize the model with the caverns (voids) and simulate the different phases during the cavern's lifetime.
- PH2 Initialization HLF+Litho - to apply the in-situ stress from the previous phase 1 to the model and introduce one cavern, or multiple caverns, initially supported by the lithostatic pressure inside the cavern.
- PH2 Litho to brine + Prod + Pinc + Pconst – to simulate the different phases during the lifetime of cavern: the construction phase, the salt production phase and the phase of pressure control. We used the same loading scenarios as in the case of the axisymmetric benchmark model (Table 7-1).

In summary, we defined 12 scenarios by combining: 3 combinations of active caverns (Table 7-1, Figure 7-3 and Figure 7-4), 1 loading scenario with 1 pressure level during the phase of pressure control (pressure increase to 90% of litho-pressure) and 4 salt creep variants (Table 4-2).

Table 7-1 Loading scenarios simulated with the plane strain model (P – pressure inside the cavern). Note that the 6 Heiligerlee caverns existing outside the central part of the cavern field are ignored in the model, i.e. they are not leached in any scenario.

Phase of cavern's lifetime	Start/End [day]	Duration [day]	Duration [yr]	Cavern pressure	Active caverns*		
Cavern construction	0-1	1		Litho-P switched to halmostatic	HK-F	HL-K	HL-C HL-E
Salt production	1-1800	1799	5.0	Halmostatic P			HL-F
P-control, P-increase	1800-2100	300	0.8	P increase to 90% of litho-P			HL-K HL-L
P-control, P-constant	2100-20000	18200	49.9	Constant elevated brine P			HL-M

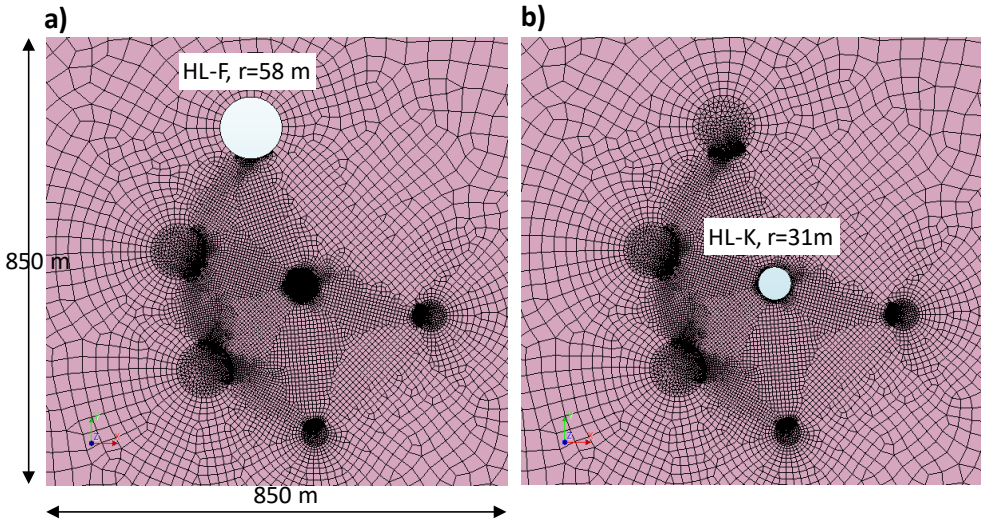

Figure 7-3: The plane strain models of single cavern with (a) the HL-F cavern and (b) the HL-K cavern (top view). The plane strain model is a horizontal slice at the mid-height of the benchmark cavern (at a depth of 1375 m).

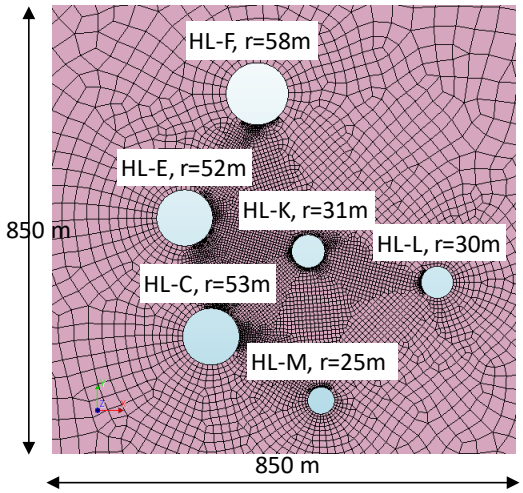

Figure 7-4: Plane strain model with six caverns (top view). The plane strain model is a horizontal slice at the mid-height of the benchmark cavern (at 1375 m depth).

7.3 Results for a single cavern and for multiple caverns

7.3.1 Single cavern model results

The plane strain model of a single cavern was used to estimate the temporal evolution of radial cavern convergence and to cross-check the axisymmetric model. Either the HL-F cavern or the HL-K cavern exists as a single cavern.

For the HL-K cavern, the agreement between both models was good (Figure 7-5 and Figure 7-6). The radii of these two caverns are similar: 27 m and 31 m, respectively. For the larger HL-F cavern, the radial convergence is about twice the convergence of the smaller HL-K cavern. This is expected, as the cavern wall convergence increases with an increase of cavern radius.

The amount of radial convergence was significantly smaller for the non-linear creep case compared to the medium linear creep case (13 cm versus 57 cm after 1800 days for the HL-K cavern, Figure 7-5 and Figure 7-6). After switching to a larger pressure in the cavern, convergence of the non-linear creep case stopped, while for the case with non-linear and linear creep combined it continued.

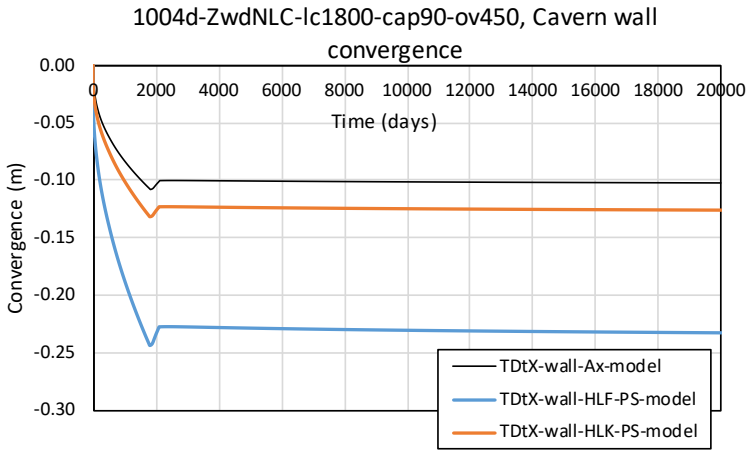

Figure 7-5: Comparison of cavern wall convergence (horizontal displacement) from the axi-symmetric model (black line, TDtX-wall-Ax-model), the plane strain model with the HL-F cavern (blue line, TDtX-wall-HLF-PS-model) and the plane strain model with the HL-K cavern (red line, TDtX-wall-HLK-PS-model). The non-linear salt creep case. The agreement is good between the caverns of similar radius (i.e. the axisymmetric model and the plane strain model with HL-K cavern).

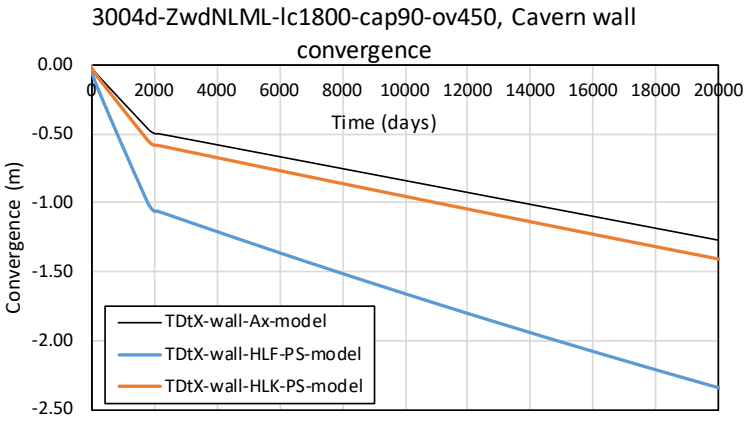

Figure 7-6: Comparison of cavern wall convergence (horizontal displacement) from the axi-symmetric model (black line, TDtX-wall-Ax-model), the plane strain model with the HL-F cavern (blue line, TDtX-wall-HLF-PS-model) and the plane strain model with the HL-K cavern (TDtX-wall-HLK-PS-model). The medium linear creep case. The agreement is good between the caverns of similar radius (i.e. the axisymmetric model and the plane strain model with HL-K cavern).

The stress profiles calculated with the axisymmetric model and the plane stress model of the HL-K cavern showed also good agreement. This is illustrated in Figure 7-7 for the case of medium linear salt creep and the controlled pressure increase to 90% of lithostatic pressure.

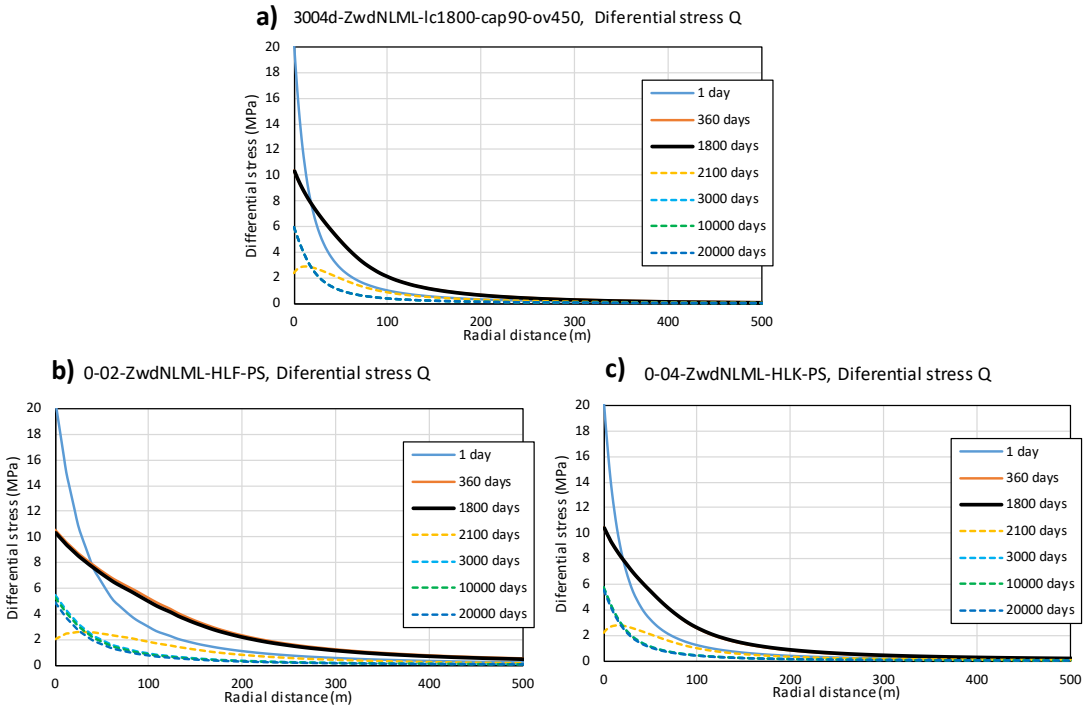

Figure 7-7: Profiles of differential stress Q with distance away from the cavern at different times from (a) the axisymmetric model (scenario 3004d), (b) the plane strain model with the HL-F cavern (scenario 0-02) and (c) the plane strain model with the HL-K cavern (scenario 0-04). The medium linear creep case. The agreement is good for the caverns of similar radius (i.e. the axisymmetric model and the plane strain model with HL-K cavern).

7.3.2 Multiple cavern model results

When six caverns were exposed to the same loading scenario (Figure 7-4, Table 7-1) the multiple caverns model showed a complex interaction among nearby caverns that affected convergence and stress evolution. Contour plots of the total displacement revealed an asymmetric (i.e. eccentric) pattern of wall convergence in a cavern affected by interference from nearby caverns (Figure 7-8).

The amount of convergence in a particular cavern was typically larger on the cavern side facing away from other caverns. In the case of HL-F cavern, for example, the amount of convergence at the point F2 (facing away) was 120 cm while at the point F1 it was 86 cm (after ~5 years of salt production, Figure 7-9). In the case of the smaller HL-K cavern, the difference in convergence between the opposite cavern sides was even larger: 96 cm at point K2 (facing away) and 16 cm at point K1 (Figure 7-9, Figure 7-10).

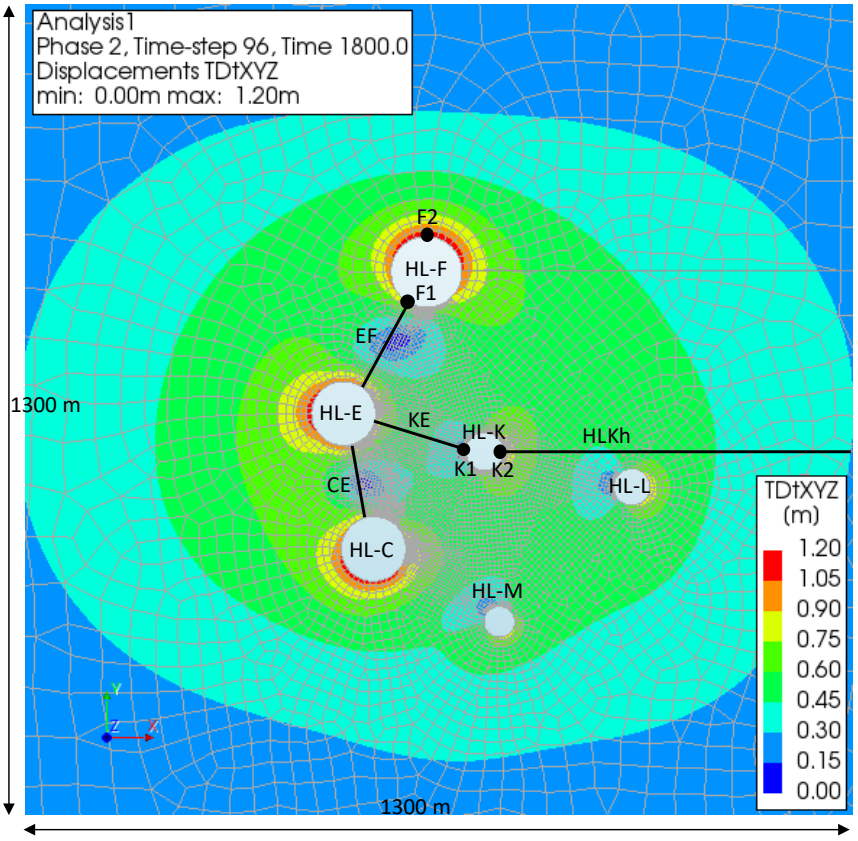

Figure 7-8: Contour plot of total displacement (TDtXYZ) after ~5 years (1800 days) of salt production from six caverns (top view).

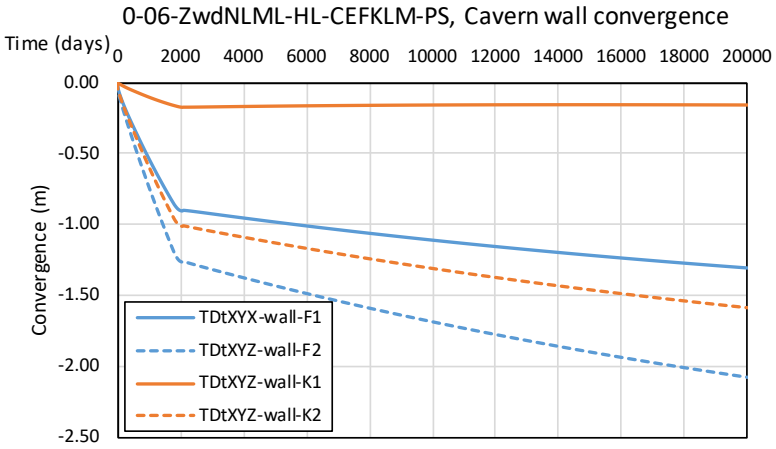

Figure 7-9: Cavern wall convergence at different observation points from the plane strain model with 6 caverns. Location of the observation points F1 and F2 (cavern HL-F), and K1 and K2 (cavern HL-K) is shown in Figure 7-8. The medium linear creep case.

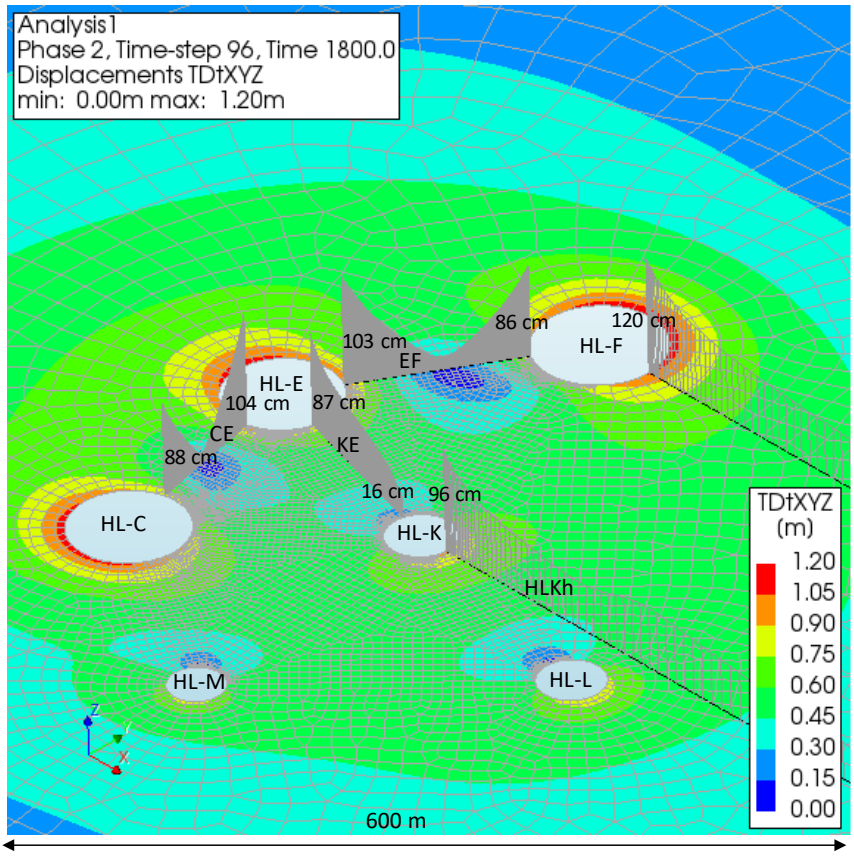

Figure 7-10: Contour plot of total displacement (TDtXYZ) after 1800 days (~5 years) of salt production from six caverns (oblique view). Displacement of cavern wall (convergence) at the location of marked profiles is written out. The medium linear creep case.

Profiles of differential stress Q along the lines connecting nearby caverns revealed the complex dynamics of stress evolution and the presence of relatively high differential stresses in the salt during the salt production phase (black and blue solid

lines in Figure 7-11). The stress profiles plotted along the HLKh-line showed the disturbance at a radial distance of ~200 m from the HL-K cavern. This is caused by salt production from the neighbouring HL-L cavern (Figure 7-11c and Figure 7-12). A contour plot of differential stress Q after ~5 years of salt production showed a complex spatial pattern of induced stress changes (Figure 7-12a).

During the subsequent phase of pressure control, the cavern pressure increased to 90% of litho-pressure, and the differential stress Q was reduced to below 2 MPa (dashed lines in Figure 7-10 and Figure 7-12b).

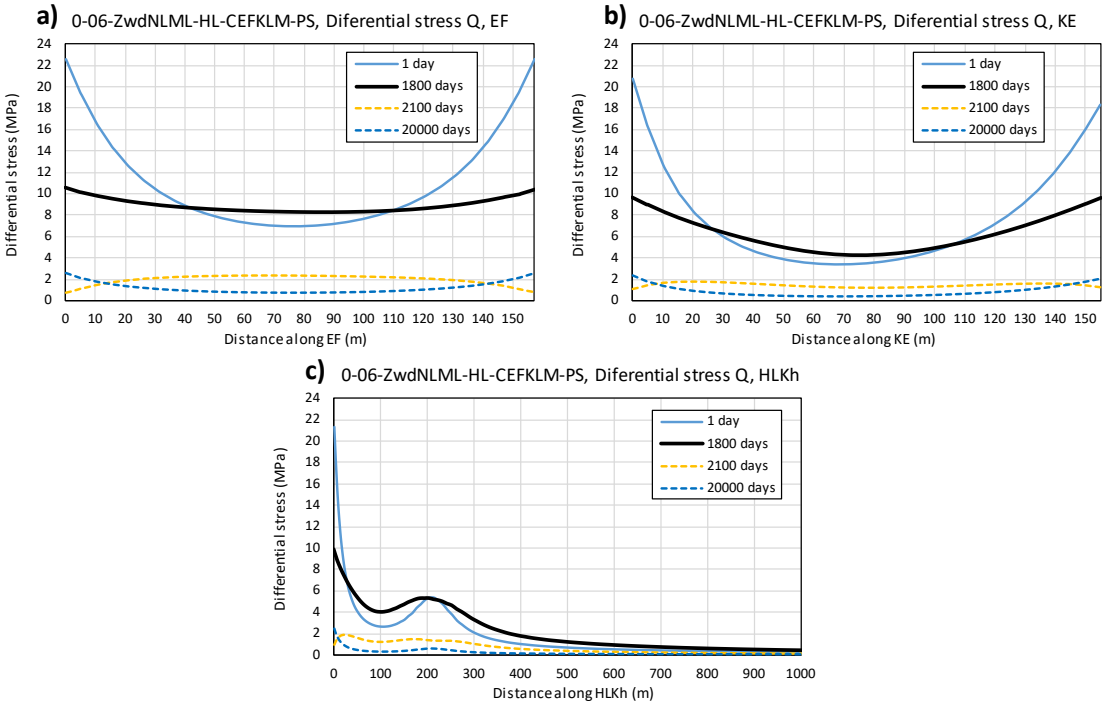

Figure 7-11Profiles of differential stress Q (a) between the caverns HL-E and HL-F (EF-profile), (b) between the caverns HL-K and HL-E (KE-profile), and (c) from the cavern HL-K away (HLKh-profile). Location of the profiles is shown in Figure 7-8. The medium linear creep case.

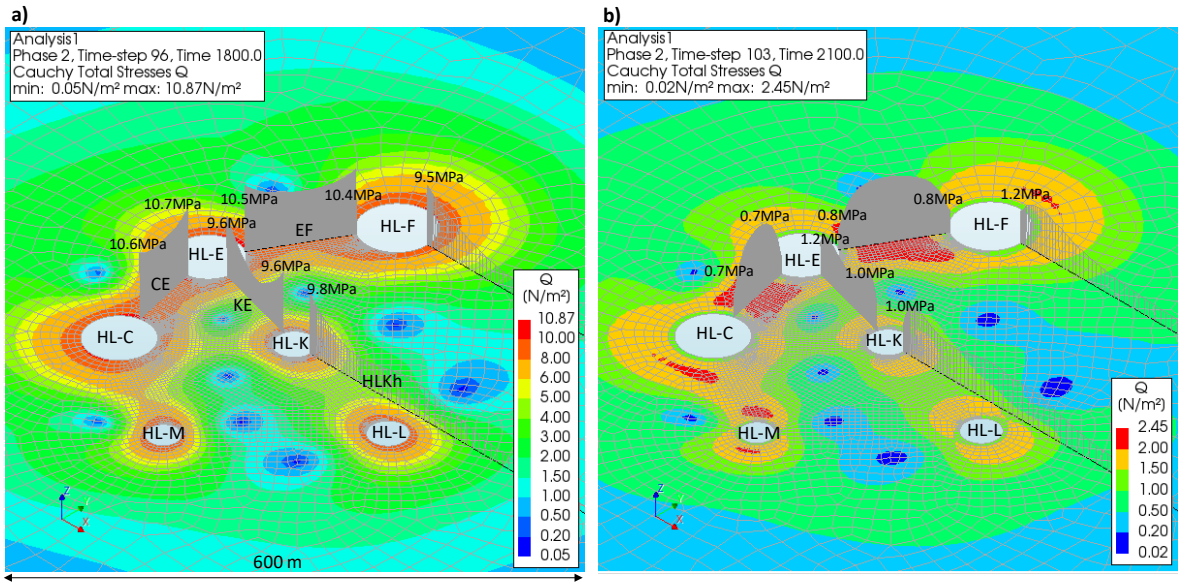

Figure 7-12: Contour plot of differential stress Q after (a) 1800 days (~5 years) of salt production from six caverns and (b) after 2100 days, at the end of controlled pressure increase to 90% of litho-pressure in six caverns (oblique view). The values in MPa's represent Q-values at cavern wall at the location of marked profiles. (N/m^2 in the legend and the title should be disregarded). The medium linear creep case. Note that the colour scale used in two plots is different.

8 Comparison with field observations

Here, we calculate subsidence rates by scaling the single cavern volume result from the numerical calculation to the actual sizes of the12 caverns in the Heiligerlee concession (Section 8.1) and then combining the deformation fields at the surface through superposition (Section 8.2). The resulting subsidence is compared to recent subsidence observations from InSAR satellite data. Finally, in Section 8.3 a preferred subsidence model is defined, to be used for forecasting purposes in Chapter 9.

8.1 Development of cavern volume (from KBB 2015)

Figure 8-1 provides an overview of the individual and total cumulative cavern volumes of the Heiligerlee salt caverns (KBB-2015 WP2). These volumes are well constrained by periodic sonar measurements. From the figure we derive the following values:

- The total cavern volume in 2015 was 33 mln m^3; this was the starting point for KBB's forecast under an extended production scenario.
- The average cavern volume over de InSAR data period (2015 – 2019) was ca. 35 mln m^3.
- For forecasting purposes (Chapter 9) we estimated the cavern volume to be 38 mln m^3 in 2022, the assumed starting year of supposed pressure control scenarios.

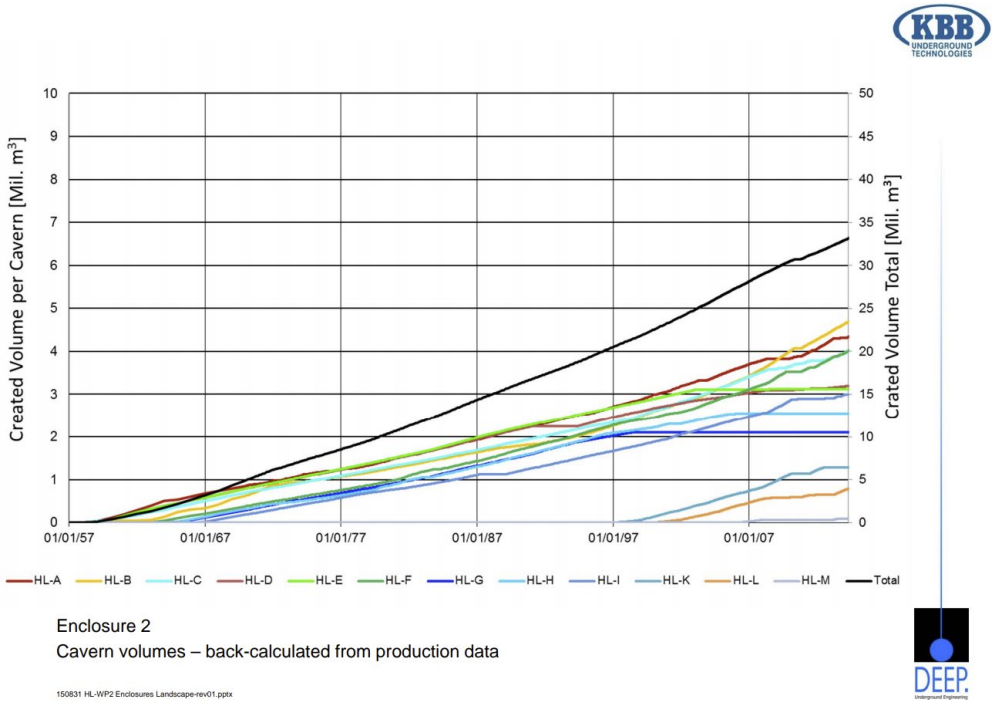

Figure 8-1:Cavern volumes of the Heiligerlee caverns since start of production up to 2015. Source: KBB, 2015.

8.2 Subsidence

8.2.1 Information sources and their uncertainties

Subsidence can be measured using different technologies. The two most common ones are optical levelling and interferometric synthetic aperture radar (InSAR), a satellite-born technique. The latter makes interferograms between radar images taken at different times[33]. With an advanced processing technique SkyGeo produced a subsidence map of the Netherlands, presenting the subsidence between January 2015 and October 2019 in terms of an average subsidence rate. Figure 8-2 and Figure 8-3 show the estimated surface movement in the north-eastern Netherlands and around the Heiligerlee salt production caverns.

Two observations must be made here. In the first place, the Heiligerlee cavern field is located at the edge of the Groningen gas field, so part of the subsidence, some 4 mm/year, originates from the depletion of the gas field. In the second place, Figure 8-3 shows the vertical surface movement from two different view angles – i.e. while in ascending or in descending pass. Because the line of sight of the satellite makes a considerable angle with the vertical direction, the presence of an east-western horizontal component introduces a systematic error. This can be seen in Figure 8-3 as an east-west shift of the location of largest movements.

Despite these and other possible processing issues, we estimate the vertical surface movement above the Heiligerlee salt cavern field caused by the salt-producing caverns at a rate of 6 ± 2 mm/year (1 sigma level) in the period January 2015 – October 2019.

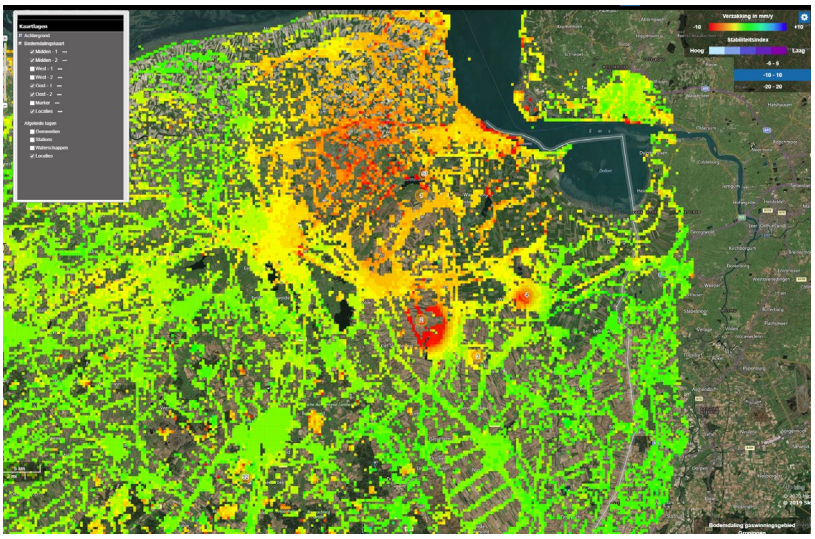

Figure 8-2: PS-InSAR-derived surface movement in NE Netherlands. Source: www.bodemdalingskaart.nl

[33] Ferretti, A. (2014). Satellite InSAR data: reservoir monitoring from space. EAGE publications

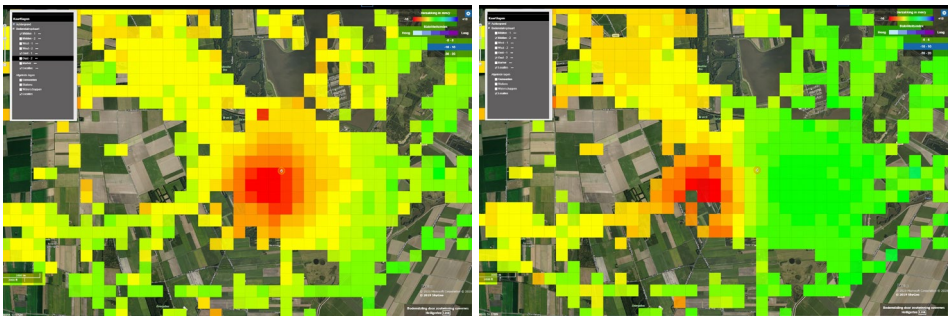

Figure 8-3: PS-InSAR-derived surface movements above the Heiligerlee salt caverns, 2015-2019. Left: With descending satellite passes. Right: with ascending satellite passes. Source: www.bodemdalingskaart.nl.

8.2.2 Consistency between model outcomes and field observations

From Section 8.1 we use the average cavern volumes in the period 2015 – 2019 and a cavern pressure that is related to production conditions (i.e. halmostatic + 20 bar). When scaled to the 1 million m^3 model cavern of Section 5.1.1, we can use DIANA-derived influence functions and estimate the subsidence rate at any time. In other words, the time-dependent subsidence bowls have been calculated by scaling the 1 million-m^3 cavern result from the numerical calculation to the actual sizes of the 12 caverns in the Heiligerlee concession and then combining the deformation fields at the surface through superposition.

Figure 8-4 shows the results. During the production phase, the NLML and the NLLL case with the 1000-m dome show maximum subsidence rates of 175 mm/yr and 35 mm/yr, respectively. With the 500-m dome, the values are 35 mm/yr and 7 mm/yr. These results are reproduced in Table 8-1. After increasing the pressure, the cavern convergence slows down; the subsidence rate is following slowly. The slow-down depends critically on the new pressure and on the magnitude of the linear creep.

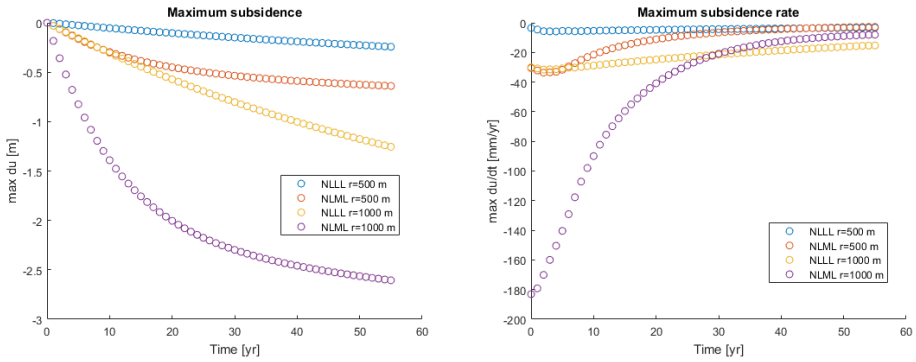

Figure 8-4: Total subsidence and subsidence rate at the centre of the subsidence bowl, for the NLML and NLLL cases. After 5 years, the cavern pressure is switched from halmostatic to 90% of the in-situ stress.

Note that Figure 8-4 was constructed based on halmostatic cavern pressure. The actual pressure (halmostatic + 20 bar) would give lightly smaller subsidence rates.

Table 8-1: Present day' subsidence rate Zmax (mm/yr) for various model variants

Radius:	**1000 m**	**1000 m**	**500 m**	**500 m**
Linear creep:	MLC	LLC	MLC	LLC
Zmax (mm/yr):	175	35	35	7

8.3 Preferred forecasting model and parameter choices for this study

From Table 8-1 we see, that the model variant with radial distance 500 meter and low linear creep comes closest to the InSAR observed rate of 6 +/- 2 mm/year; the other variants all give (much) faster subsidence rates at the deepest point.

We also note, that the calculated subsidence rates - in a fair approximation - are linear both in the radial distance and in the linear creep (cf. Chapter 4: ratio between MLC and LLC is approximately 6). The result is that the combined nonlinear and low linear creep model is our preferred model for forecasting purposes, to be used in Chapter 9.

9 Forecasting

9.1 Pressure control scenarios

During production, the pressure at the cavern top is of the order of 60% of the virgin in-situ lithostatic stress. As a result, the radial stresses at the cavern wall are reduced and the cavern volume converges due to salt creep. If the wells to the caverns would be completely closed and no pressure control installed, the salt creep and the associated cavern squeeze will result in an increase of the brine pressure. Because the brine density is lower than the rock salt density, the brine pressure at the cavern top may even exceed the virgin stresses. This is clearly an unwanted situation, since a cavern overpressure can induce uncontrolled upward cavern growth or even the creation and propagation of hydraulic fractures.

Therefore, the scenarios that are envisaged are pressure control scenarios. Maintaining halmostatic pressure is the one end member option. Because of the risk of overpressure, we have taken the other end member at 90% of the virgin lithostatic stress. We also investigated scenarios with pressures between those values (i.e. 70 and 80% of lithostatic pressure).

9.2 Subsidence profiles

In Section 8.3 we have selected the 500-m dome radius and the Low Linear creep model, based on the InSAR data, as the model to forecast subsidence.

Figure 9-1 presents the areal distribution of the subsidence after 50 years of shut-in, for these the cases with halmostatic pressure and with 90% pressure, after integration of the contribution of all the salt caverns. The shape of the subsidence rate maps is somewhat sharper for the 90% case since the increase in pressure results in a concentration of the subsidence closer to the centre of the subsidence bowl.

Figure 9-2 presents the evolution of the deepest point of the subsidence bowl for the 4 shut-in cases considered. Of particular interest is the scenario in which after cessation of salt production cavern pressures would be put at a control level of 90% of lithostatic. Our modelling shows, that in 50 years the subsidence rate would gradually decrease with a factor close to 2 with respect to the halmostatic case (cf. Table 9-1). This time-dependence is a combined effect of the dynamics of the decreasing cavern volume, the time dependence in the connection between convergence volume rate and subsidence rate, and the change of subsidence bowl shape.

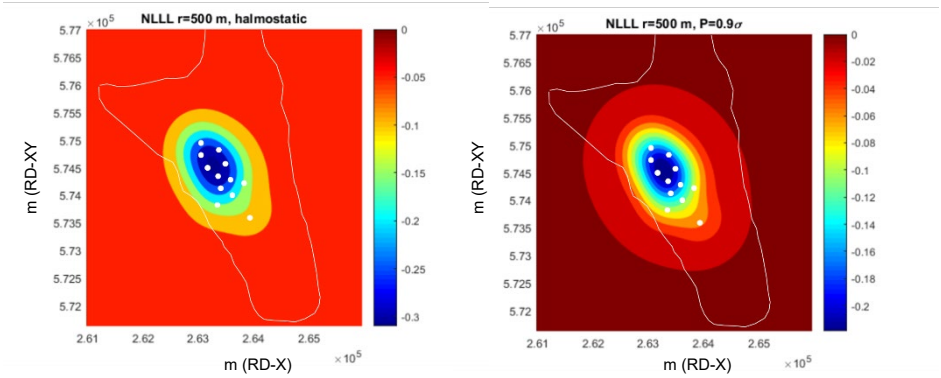

Figure 9-1: Contours of total subsidence [in m] during 50 years of shut-in, for the 500-m salt dome with the NLLL creep law, for the complete cavern field. Left: for halmostatic cavern pressure. Right: cavern pressure increased to 90% of the virgin stress magnitude. The white dots show cavern locations. The white line represents the outline of the Winschoten dome at -1.500m

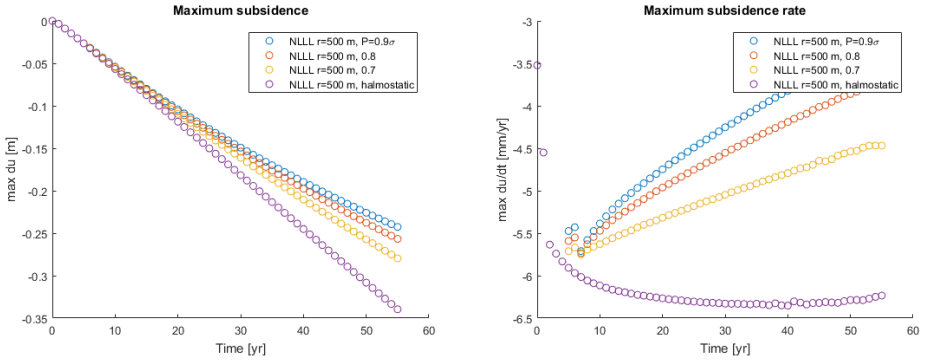

Figure 9-2: Maximum subsidence (left) and subsidence rates [mm/yr] for the 500-m salt dome with the NLLL creep law, for different levels of shut-in pressure. Shut-in started after production at halmostatic pressure during 5 years.

Table 9-1: Modelled forecast subsidence rate and total subsidence during shut-in and during production plus shut-in.

Pressure control level:	**halmostatic**	**70% of lithostatic**	**80% of lithostatic**	**90% of lithostatic**
Subsidence rate after 3 years of shut-in	6.0 mm/yr	5.7 mm/yr	5.7 mm/yr	5.7 mm/yr
Subsidence rate after 50 years of shut-in	6.2 mm/yr	4.5 mm/yr	3.7 mm/yr	3.3 mm/yr
Total subsidence during 50 years shut-in	31±11 cm	25±8 cm	23±8 cm	22±7 cm
Total subsidence after production and shut-in, in 2072	49±11 cm	43±8 cm	41±8 cm	40±7 cm

9.3 Summary of subsidence forecasts (50 years ahead)

Figure 9-3 shows a condensed summary of the results from this study in terms of the deepest point of the subsidence bowl (Zmax) due to salt cavern operations only for various cases, as discussed below.

Business as usual

As a reference the curve 'KBB 2015 report (trend)' represents the development of Zmax, if the operational production plan of Akzo would be followed, that was presented to KBB for their 2015 subsidence forecast (KBB 2015, WP3). The accelerating trend in that curve stems from the steadily increasing open cavern volume, that KBB expects to further grow by some 50% from 2015 to 2050. At that point in time, Zmax would have increased from 15 to 33 cm.

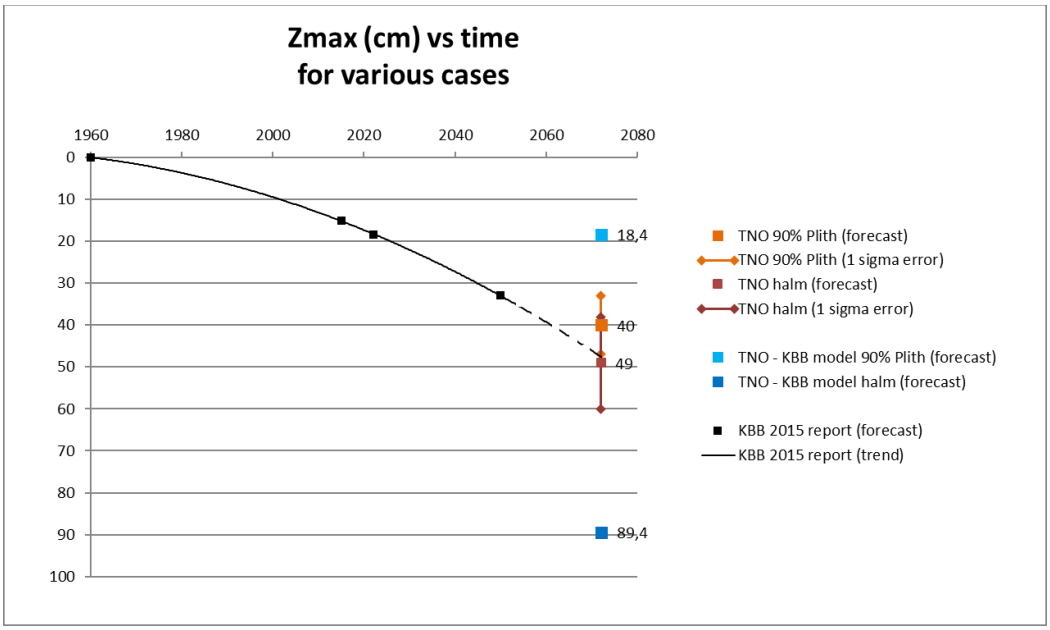

Figure 9-3: Subsidence at deepest point (Zmax) caused by the Heiligerlee salt cavern field operation for various cases. The TNO-calculated cases include indicative error bars

In the – yet hypothetical – case the salt mining would be stopped in 2022, and all caverns would simultaneously be put under pressure control, two other cases are shown:

Pressure control at halmostatic pressure

This simply means leaving the wells open to atmosphere: the excess pressure due to water injection (20 bar) would vanish. It is observed, that in this case the KBB 'power law only salt creep' model (data point 'KBB halm') would lead to some 89 cm subsidence in 2072. Note that – according to the n = 5 power law - lowering the cavern pressures by only 20 bar causes an increase in the convergence rate, and thereby subsidence rate, by a factor of ca. 2.5.

However, the TNO model including linear salt creep (data point 'TNO halm') leads to significantly less subsidence in 2072: 49±11 cm. The difference is due to the introduction of linear creep in the TNO model.

Pressure control at 90% of lithostatic pressure

This scenario sits at the other end of the range of pressure control scenarios considered in this study. Here, the difference in Zmax between the KBB power law only model (data point 'KBB 90% lith) and the TNO model (data point 'TNO 90% lith') is opposite to the halmostatic case. In fact, according to the 'power law only' creep model subsidence would immediately stop and stay at the 2022 level of Zmax = 18.4 cm, while according to the TNO model subsidence would continue and reach 40±7 cm in 2072. This difference is also attributed to the introduction of linear salt creep in the TNO model.

9.4 Discussion

9.4.1 Interpretation

We interpret the subsidence results presented above as follows. At relatively high pressure differentials between the internal cavern brine pressure and the lithostatic pressure in the salt rock mass, the power law term in the Ellis model strongly dominates over the linear creep term. This is the case in pressure control at halmostatic level. However, if the pressure differentials are controlled at a relatively low level, the contribution of linear creep gets more important, to the extent that it may even dominate the cavern convergence – like in the 90% of lithostatic case.

9.4.2 Uncertainties

Salt creep model

Salt creep is the driving force for cavern convergence and subsidence. The key parameter in our analysis has been the contribution of linear creep in the two branch Ellis model. We have considered the existence of linear creep as a given and treated 'power law only' as an unrealistic model at low deviatoric stresses (<10 MPa). Moreover, our study shows that under 'power law only' salt creep behaviour the stress field in the geomechanical system does not reach steady state at relevant time scales (consistent with literature[34]), which further complicates forecasting.

Based on literature on experiments (cf. Chapter 4), the uncertainty in the linear creep has been expressed in an *a priori* range [LLC – MLC – HLC] spanning a factor of 30 between the low and high value.

DIANA FEM

The DIANA model has been constructed as a 1 mln m^3 model cavern within a geological setting and mechanical properties representative for the Heiligerlee caverns. It has been tacitly assumed, that the volumetric convergence rate linearly scales with the cavern volume. This scaling rule was applied to treat the actual Heiligerlee caverns, that have present day volumes ranging from 1 to some 4 mln m^3 (cf. Table 2-1).

[34] Manivannan, S. & Bérest, P. (2019): Transient Closure of a Cylindrical Hole in a Salt Formation Considered as a Norton–Hoff Medium." *Rock Mechanics and Rock Engineering* 52.8, 2701-2707.

The only aspect that was varied in the architecture of the DIANA model, is the characteristic radial distance [range 0.5 – 5.0 km] of a cavern to a salt flow boundary, meant to represent the finite size of the Winschoten salt dome in contact with a geological non viscous 'side burden' (cf. Figure 2-2).

Preferred subsidence model
The TNO subsidence forecast presented above stems from a single 'preferred' model (Chapter 8), that was scaled to the 'present day' subsidence rate observed from InSAR (6 +/- 2 mm/year) from salt operation only. Note that the contribution from the Groningen gas field below the Heiligerlee cavern system complicates the subsidence data analysis. That 'preferred' model is characterized by a 0.5 km radial distance to a salt flow boundary combined with low linear creep (LLC). These parameter values happen to be at the very low end of both model parameter ranges investigated in our study. Other combinations of values for radial distance and linear creep derived from the uncertainty ranges lead to a (much) faster subsidence rate, and therefore do not explain the observed subsidence rate derived from InSAR, even when including the uncertainty on the InSAR data themselves.

As the salt dome and cavern layout map in Figure 2-2 shows, 0.5 km is in fact the shortest distance of only some of the Heiligerlee caverns to the western flank of the Winschoten dome; the average distances of the Heiligerlee caverns to the edges of the Winschoten dome are larger: ca. 1 km in east-west direction, and several km's in north-south direction. Therefore, an interpretation of the 0.5 km radius in terms of the geological structure of the salt dome is not straightforward. The uncertainty analysis above suggests that another than the preferred model could explain the observed subsidence rate equally well. In particular, one may consider a combination of a shorter than 0.5 km radial distance and higher than low linear creep (LLC). It is also possible that the larger caverns at a distance of 1 km from the dome edge scale to the smaller model cavern at 500 m distance.

Potential alternative model/ interpretation
Prof. Chris Spiers has indicated (pers. com. 30-11-2020), that linear salt creep at the depth of the Heiligerlee caverns for plausible physical reasons[23] is likely to be non-active at deviatoric stresses below a value in the range 0.07 – 0.7 MPa. Based on our DIANA model of a 1 mln m^3 cavern, these values translate into a spatial range for that threshold between 500 and 150 m under production cavern pressure conditions (i.e. halmostatic + 20 bar). Here it should be noted, that most of the Heiligerlee caverns actually are larger than our model cavern (cf. Table 2-1), with a cavern radius that is up to a factor 2 larger than that of our model cavern. For those caverns a certain level of deviatoric stress will be reached at twice the distance from the cavern compared to our model cavern. Therefore, for the larger caverns the threshold levels for linear creep mentioned above would be reached at distances in the order of 1000 – 300 m.

This opens the possibility to interpret the salt rheological behaviour in the Heiligerlee system in terms of a two branch Ellis model at micro-scale, restricted by a threshold in de deviatoric stress at radial distances below 500 m, that still honours the higher values for the linear creep derived from various experiments on salt samples from the same Zechstein 2 sequence as in Winschoten/ Heiligerlee. This would make the interpretation of the rheology at system level independent of the

geological structure of the salt(dome), and rather refer to an intrinsic dynamic property of the system.

10 Closing remarks and recommendations

As requested by SodM, this study was aimed at studying the long-term effects of a soft shut-in ‘pressure controlled’ strategy for the abandonment of the Heiligerlee salt caverns field.

Justification of our workflow
By introducing a combination of power law and linear salt creep, this study provides insight into the long-term subsidence related to cavern closure under pressure control scenarios. It was shown that linear salt creep will create ‘futures’ for cavern convergence and associated subsidence, that – depending on the pressure control level chosen - are markedly different from the case in which linear creep is neglected altogether.

In the original modeling strategy, we had chosen for a combination of numerical and analytical tools: numerical tools to describe in sufficient detail the caverns and their relevant geomechanical environment, and analytical tools to extend the outcomes of the numerical modeling to long term full closure, far beyond the domain were numerical models are capable of forecasting.

However, during the project it became clear that application of linear salt creep in a laterally unbounded salt layer resulted in unrealistic subsidence profiles (with uplift in the center of the bowl) that are not observed by geodetic information at the Heiligerlee cavern field. In response to that observation, we have introduced a finite lateral spatial dimension of the salt formation (dome) into the numerical modeling, of the order of the typical dimensions in the Heiligerlee case (ranging from 0.5 to 5 km). Only then realistic subsidence profiles could be obtained.

As a consequence, the analytical expression for cavern convergence, driven by a combination of power law and linear salt creep, could not be used as planned. For the same reason, the results of our 2D multi cavern model could not be used to study cavern convergence interactions as planned.

Another consequence was, that we had to fully rely on the single cavern FEM model for both cavern convergence and the generation of influence functions (the time dependent response of subsidence on cavern convergence). Moreover, for these practical reasons, the time horizon for forecasting subsidence under pressure control scenarios was limited: we have presented results for a ca. 50 year ahead period. Nevertheless, we feel that a 50 years ahead period will serve to monitor the subsidence behavior and in doing so reduce the uncertainty that exists on the outcome of our modeling.

Forecast
A general observation is, that introducing linear creep into the geomechanical modelling does significantly relax the dependence of convergence on cavern pressure, that would occur under a power law only assumption.
The interaction between caverns, as modelled in this report, will probably turn out to be significantly less, when a threshold in the spatial action of linear creep is introduced.

Uncertainties
We have quantified the impact of parameter uncertainty in our preferred forecasting model. For a large part, that uncertainty is caused by the uncertainty on the subsidence actually generated to date from the Heiligerlee project.

As to model uncertainty: we do feel, that uncertainty in the actual behavior of the salt body in the Winschoten dome in response to salt mining (and storage) activities may not be sufficiently captured yet:

- We have tacitly assumed, that results from experimental creep test on small salt samples, combined with field scale material balance and echometric data, are representative for the effective behavior of the full salt dome body. But convergence rates are so low, that convergence can only indirectly be determined, i.e. through subsidence (which is the objective of this study);
- Although the lab results from various wells and depth intervals do suggest a relatively uniform effective overall behavior, the impact of heterogeneities cannot be ruled out and is presently unknown;
- Our modeling has neglected the effect of a cooling effect of the injected fluid on the mechanical behavior of the salt surrounding the caverns; this may have an effect on the 'history matching'; the effect is expected to decrease over time in a pressure control mode, when temperature balances again.

Within the framework of our forecasting model, there seems to be a trade-off between the contribution of linear salt creep and the lateral spatial extent of the action of linear salt creep. The combination of Low linear creep and a 500-meter effective radius for the salt dome was found to comply favourably well with the observations. Should the effective radius be an intrinsic salt creep feature, then this parameter combination is not unique: a combination of higher values for linear creep with a smaller radius might explain the convergence and subsidence rates equally well. In fact, applying the range provided by prof. Spiers (0.07 – 0.7 MPa, pers.comm 30-11-2020) to the Heiligerlee case corresponds to spatial ranges for linear creep in the order of between 500 and 150 m. Therefore, it cannot be excluded that the contribution of intrinsic linear creep is stronger than assumed in the Low case.

Finally, in his review prof. Spiers has pointed at mechanisms that are not included in the Ellis creep law formulation, but may lead to acceleration of the salt creep:

- Dynamic recrystallization, occurring at strains > 0.1: we have verified, that our FEM results for the preferred model do not exceed that strain value;
- Dilatancy: acceleration of creep due to permeation of brine in the dilated zone (not further investigated here).

Recommendations
We like to stress that the modelling assumptions leading to our results need further scientific confirmation, both theoretically and from experiments, and thus further research. They possibly touch at the resolution of a long-standing discussion of the role of linear salt creep at various spatial and time scales (lab, mining engineering, tectonics).

This has led us to the following recommendations:

- Perform a critical scientific review as to the underlying modelling assumptions. The review should in particular target the importance of linear salt creep, including the physical threshold for the deviatoric stress for linear creep that is supposed to exist from a fundamental physics point of view.
- Perform an inverse study on the geodetic signals from the Heiligerlee cavern histories (InSAR and benchmarks) in order to unravel the contributions from salt cavern related operations, the Groningen gas field and other (autonomous) sources. Such a study should target to better determine the cavern squeeze rate along with the driving geomechanical parameters. This would enhance the history match of the geomechanical modelling, especially since in the Heiligerlee case convergence volume is not with any practical accuracy measurable in-situ or derived from mass balance considerations.
- Consider the added value and the practical feasibility of the ‘soft shut-in’ method approach investigated here when compared to the traditional hard shut-in method.
- Develop a monitoring program, that is able to validate (or reject) the subsidence projections made in this study, in case a soft shut-in is applied to the Heiligerlee caverns.

11 References

[2] Rokahr, R.B., Hauck, R., Staudtmeister, K., Zander-Schiebenhofer, D., Crotogino, F. & Rolfs, O. (2002). High pressure cavern analysis. SMRI report no. 2002-2-SMRI, 88 p.

[3] Pruiksma, J.P. (2005). Shut-in gedrag en stabiliteit FRISIA caverne, FEM berekeningen en kruipgedrag. Delft: Deltares, Report No. CO-400132-0006

[4] Lux, K.-H. & Wolters, R. (2010). Untersuchung der konvergenzinduzierten zeitlichen und räumlichen Soleinfiltration aus der Kaverne BAS-3 in das anstehende Steinsalzgebirge, Clausthal

[5] Bérest, P. & Brouard, B. (2003). Safety of Salt Caverns Used for Underground Storage Blow Out; Mechanical Instability; Seepage; Cavern Abandonment. Oil & Gas Science and Technology 58(3):361-384. DOI: 10.2516/ogst:2003023

[6] Fokker, P.A. (2018), "Managing pressures in Nedmag caverns to prevent brine leakage during the mining and bleed-off phase and an evaluation of post abandonment cavern behaviour." (available from www.nedmag.nl)

[8] Akzo-Nobel 2004, Caverneveld Heiligerlee doorsnede 1

[9] KBB (2018), Prediction of Subsidence above Caverns at Heiligerlee, The Netherlands Operation Phase Report on WP2: Applied Subsidence Model, KBB for Akzo-Nobel (31-8-2015)

[10] KBB (2018), Prediction of Subsidence above Caverns at Zuidwending, The Netherlands Operation Phase Report on WP2: Applied Subsidence Model, KBB for Akzo-Nobel (31-8-2015)

[11] IfG (2016), Rock Mechanical Modelling (incl. history and surrounding caverns) of the Nitrogen Storage Cavern HL-K at Heiligerlee, The Netherlands, IfG for Gasunie (28-6-2016)

[14] Sobolik, S.R. & Ehgartner, B.L. (2012). Analyzing large pressure changes on the stability of large-diameter caverns using the M-D model. Mechanical Behavior of Salt VII - Proceedings of the 7th Conference on the Mechanical Behavior of Salt. 321-329. 10.1201/b12041-44.

[15] Urai, J.L., Spiers, C.J., Zwart, H.J. & Lister, G.S. (1986): Weakening of rock salt by water during long-term creep. Nature 324 (6097), pp. 554–557.

[16] Spiers, C.J., Schutjens, P.M.T.M., Brzesowsky, R.H., Peach, C.J., Liezenberg, J.L. & Zwart, H.J. (1990): Experimental determination of constitutive parameters governing creep of rocksalt by pressure solution. In: Knipe, R.J., Rutter, E.H. (Eds.), Deformation Mechanisms, Rheology and Tectonics. Geological Society, London, Special Publications, 54, pp. 215–227.

[17] Breunese, J.N., van Eijs, R.M.H.E., de Meer, S. & Kroon, I.C. (2003). Observation and prediction of the relation between salt creep and land subsidence in solution mining—The Barradeel case, paper presented at SMRI Conference, Chester.

[18] Wallner, M., Lux, K.H., Minkley, W., & Hardy Jr, H.R. (Eds.). (2017). The mechanical behavior of salt – Understanding of THMC processes in salt: Proceedings of the 6th Conference on the Mechanical Behavior of Salt. Hannover, Germany, 22–25 May 2007. CRC Press.

[19] Wang, L., Bérest, P. & Brouard, B. (2015). Mechanical behavior of salt caverns: Closed-form solutions vs numerical computations. Rock Mech. Rock Eng. 48: 2369-2382.

[20] Lux, K.-H. (1984): Gebirgsmechanischer Entwurf und Felderfahrungen im Salzkavernenbau (Ferdinand Enke Verlag, Stuttgart 1984)

[21] IfG (2006): Rock mechanical investigations on rock salt from cavern well BAS4, IfG for ESCO / Frisia Zout BV (17-10-2006)

[22] Van Noort, R., Visser, H.J.M. & Spiers, C.J. (2008): Influence of grain boundary structure on dissolution controlled pressure solution and retarding effects of grain boundary healing. J. Geophys. Res. Solid Earth 113 (3), pp. 1–15.

[23] Desbois, G., Urai, J.L. & De Bresser, J.H.P. [2012]: Fluid distribution in grain boundaries of natural fine-grained rock salt deformed al low differential stress (Qom Kuh salt fountain, central Iran): Implications for rheology and transport properties, Journal of Structural Geology (2012) pp. 1-16.

[24] Peach, C.J., Spiers, C.J. & Trimby, P.W. (2001): Effect of confining pressure on dilatation, recrystallization, and flow of rock salt at 150°C. J. Geophys. Res. 106 (B7), pp. 13,315-13,328.

[25] Ter Heege, J.H., De Bresser, J.H.P. & Spiers, C.J. (2005a): Rheological behaviour of synthetic rocksalt: The interplay between water, dynamic recrystallization and deformation mechanisms. J. Struct. Geol. 27 (6), pp. 948–963.

[26] Ter Heege, J.H., De Bresser, J.H.P. & Spiers, C.J. (2005b): Dynamic recrystallization of wet synthetic polycrystalline halite: Dependence of grain size distribution on flow stress, temperature and strain. Tectonophysics 396 (1–2), pp. 35–57.

[27] IfG (2007), Rock mechanical investigations on rock salt from the Zuidwending gas storage site. Report number 11/2007.

[28] Orlic B. & Wassing B.B.T. 2013. A study of stress change and fault slip in producing gas reservoirs overlain by elastic and viscoelastic caprocks. Rock Mechanics and Rock Engineering. 46:421-435.

[29] Fokker, P.A. & Osinga, S. (2018). On the use of influence functions for subsidence evaluation. In *52nd US Rock Mechanics/Geomechanics Symposium*. American Rock Mechanics Association.

[30] Cornet, J., Dabrowski, M. & Schmid, D.W. (2017). Long-term cavity closure in non-linear rocks. Geophysical Journal International, 210(2), 1231-1243.

[31] Van Keken, P.E., Spiers, C.J., Van den Berg, A.P. & Muyzert, E.J. (1993). The effective viscosity of rocksalt: implementation of steady-state creep laws in numerical models of salt diapirism. Tectonophysics, 225(4), 457-476.

[32] Urai, J.L., Schléder, Z., Spiers, C.J., & Kukla, P.A. (2008). Flow and transport properties of salt rocks. *Dynamics of complex intracontinental basins: The central European basin system*, 277-290

[33] Ferretti, A. (2014). *Satellite InSAR data: reservoir monitoring from space*. EAGE publications.

[34] Manivannan, S. & Bérest, P. (2019) Transient Closure of a Cylindrical Hole in a Salt Formation Considered as a Norton–Hoff Medium. Rock Mechanics and Rock Engineering 52.8, 2701-2707.

12 Signature

Utrecht, 28 July 2021 TNO

Drs. J.A.J. Zegwaard
Head of Advisory Group for Economic Affairs